



Contents lists available at ScienceDirect

Journal of Fluids and Structures

journal homepage: www.elsevier.com/locate/jfs

Propulsion and energy harvesting performances of a flexible thin airfoil undergoing forced heaving motion with passive pitching and deformation of small amplitude

R. Fernandez-Feria^{*}, J. Alaminos-Quesada

Fluid Mechanics Group, Universidad de Málaga, Dr Ortiz Ramos s/n, 29071 Málaga, Spain



ARTICLE INFO

Article history:

Received 13 October 2020

Received in revised form 15 January 2021

Accepted 16 February 2021

Available online xxxx

ABSTRACT

The fluid–structure interaction in a foil undergoing prescribed heave with passive pitching and flexibility about any pivot is formulated in the linear inviscid limit using a quartic approximation for the deflection. The resulting system of three algebraic equations is valid for arbitrary mass and stiffness distributions of the foil. The small pitching and deformation amplitudes result linearly from two of the equations, while the third equation provides the force at the pivot point that generates the heaving motion, and hence the power input. This general formulation allows to analyze jointly both the propulsion and the energy harvesting problems for this class of flapping foils. In the first case, the thrust force is readily obtained from the prescribed heave and the resulting pitching and deformation, and consequently the propulsive efficiency once the power input is computed. In the second problem, the energy may be harvested by linear and/or torsional dampers at the pivot point, so that the efficiency of the system is readily computed once the pitch motion and the power input are obtained. Thus, the present work allows for a depth parametric survey and analysis of these two physical problems. The best performance is usually obtained around the first natural frequency of the fluid–structure system, which is obtained here by minimizing an algebraic function. The formulation is validated by reproducing some previous results for both problems, most of them obtained numerically for rigid foils and without the simplicity nor the richness in the parameter space of the present formulation. The parametric range for which flexibility maximizes the propulsion and the energy harvesting efficiencies in relation to an otherwise identical rigid-foil system is analyzed.

© 2021 Elsevier Ltd. All rights reserved.

1. Introduction

Flapping-foil systems with prescribed heave motion and passive pitch have been shown to be able to improve its propulsive performance in relation to heaving-only wings or fins (Moore, 2014, 2015; Asselin and Williamson, 2019), as well as its energy harvesting efficiency when used as flapping-foil turbines (Boudreau et al., 2019a,b), particularly for rigid foils. The improvement may be quite substantial if the torsional spring constant allowing the passive pitch is optimally selected in relation to the other structural and kinematic parameters of the flapping foil, which are obviously in different ranges depending on whether it is a propulsor or a energy harvester. These optimal values are usually related to resonant frequencies of the system (Alben, 2008; Moore, 2014, 2015; Asselin and Williamson, 2019).

^{*} Corresponding author.

E-mail addresses: ramon.fernandez@uma.es (R. Fernandez-Feria), jalaminos@uma.es (J. Alaminos-Quesada).

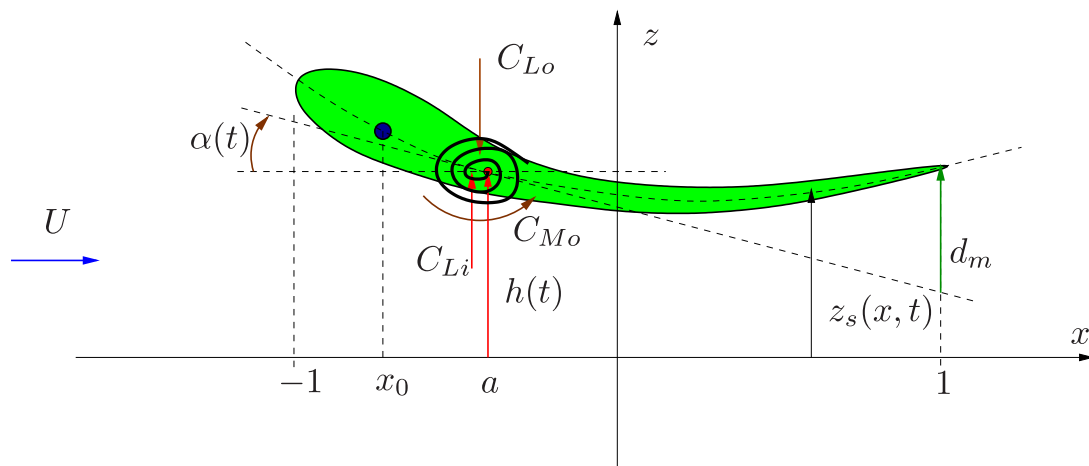


Fig. 1. Schematic of the motion of the plate (nondimensional).

In the present work we propose a general theory which yields analytical solutions for the propulsive or the energy harvesting performance of these flapping-foil systems with passive pitching and passive deformation in the limit of small flapping and deformation amplitudes and high Reynolds numbers, so that the two-dimensional, linear potential theory may be used for the fluid flow, and the Euler–Bernoulli beam equation for the fluid–structure interaction (FSI). Otherwise, the problem is formulated with the greatest generality: for any foil mass distribution and arbitrary pivot point location, so that any distance between the center of mass and the pivot point is allowed, any stiffness distribution, and of course, for any spring stiffness and operating frequency. To that end, general results recently obtained from the vortical impulse theory for the lift, thrust, moment and flexural moment exerted by the fluid on a foil undergoing arbitrary pitching and heaving motions coupled with arbitrary quartic flexural deformations are used (Alaminos-Quesada and Fernandez-Feria, 2020; Fernandez-Feria and Alaminos-Quesada, 2021). The limitation to (small amplitude) quartic deformations restricts the theory to include only the first resonant frequency of the system, but, as shown by Alben (2008) from a general linear potential flow theory, and by Moore (2015) including passive pitching like the present one, the maximum possible thrust coefficient is always achieved by the flexible foil operating at or near its first resonance. Though Moore’s theory contains the infinite resonant modes of the system, the problem has to be solved numerically, while here the problem is reduced to solving a system of just three algebraic equations, which also covers the analogous energy harvesting problem when appropriate values of some parameters are selected. These analytical expressions are obtained here because the different formulation and because the aforementioned analytical expressions for the fluid forces and moments derived from the vortex impulse theory.

The first resonant mode is obtained from the determinant of a 2×2 matrix containing all the relevant dimensionless parameters governing the system, capturing exactly well known results when FSI is neglected. The theory is also favorably compared with previous theoretical, numerical and experimental results for flapping foils with passive pitching, especially for rigid foils. The role played by passive deformation of the foil is characterized in both the propulsion and the energy harvesting problems when the foil-mass distribution is constant, so that the center of mass coincides with the mid chord point, but analyzing the effect of varying the pivot point location. In all cases, the optimal performance is related to resonant modes of the system, as previously found for similar flapping systems (Alben, 2008; Michelin and Llewellyn Smith, 2009; Alben et al., 2012; Moore, 2014, 2015; Floryan and Rowley, 2018).

2. Formulation of the problem

We consider a two-dimensional (2D) foil of chord length c immersed in an incompressible and nearly inviscid flow with constant free-stream speed U along the x -axis. We use nondimensional variables scaled with the half-chord length $c/2$ and the velocity U . A harmonic heaving motion along the z -axis, $h(t)$, is imposed through a (dimensionless) force C_{Li} on a given point $x = a$, which will be described below with more detail. The foil may undergo a superimposed passive pitching motion with angle $\alpha(t)$ around this pivot axis, where the plate is elastically supported with a torsional spring. Additionally, it may also be supported by a linear spring and by linear and torsional dampers in the case that the system is used to extract energy from a current. To formulate these last elements in a general form we include them within general (dimensionless) output force and moment, C_{Lo} and C_{Mo} , respectively, which will be modeled below (see Fig. 1).

The amplitudes of the heaving and pitching motions are assumed small compared with the chord length c , i.e., $|h| \ll 1$ and $|\alpha| \ll 1$, so that the foil, and every point of the trail of vortices that it leaves behind, may be considered to be on the plane $z = 0$ in first approximation, with the plate extending from $x = -1$ to $x = 1$. In addition, we shall consider

the flexibility of the foil assuming a large stiffness, so that its deflection in relation to a rigid foil is also very small. Thus, the motion of the plate is governed by the Euler–Bernoulli beam equation, which in dimensionless form can be written as (e.g., Moore, 2017; Floryan and Rowley, 2018; Fernandez-Feria and Alaminos-Quesada, 2021)

$$2R \frac{\partial^2 z_s}{\partial t^2} + \frac{2}{3} \frac{\partial^2}{\partial x^2} \left(S \frac{\partial^2 z_s}{\partial x^2} \right) + C_{Lo} \delta(x - a) + 2C_{Mo} \delta'(x - a) = \Delta C_p + C_{Li} \delta(x - a), \quad (1)$$

where $z_s(x, t)$ is the displacement in the z direction of the foil's centerline, the dimensionless time t is scaled with $c/(2U)$ and $\Delta C_p(x, t)$ is the pressure difference between the lower and upper sides of the foil, $\Delta p = p^- - p^+$, scaled with ρU^2 , where ρ is the fluid density. To this distributed pressure force exerted on the foil by the moving fluid, we have added to Eq. (1) some punctual forces and moment actuating locally at $x = a$. Thus, $C_{Li}(t)\delta(x - a)$ is the dimensionless force per unit span, scaled with $\rho U^2 c/2$, that generates the prescribed heaving motion, where C_{Li} has to be computed as a part of the solution of the present problem and where $\delta(x - a)$ is Dirac's delta function centered at $x = a$. On the other hand, $C_{Lo}\delta(x - a)$ and $C_{Mo}\delta'(x - a)$ are the dimensionless force and torque per unit span, scaled with $\rho U^2 c/2$ and $\rho U^2 c^2/2$, respectively, transmitted to the linear and torsional springs (and dampers) at $x = a$ by the foil, where δ' is the derivative of Dirac's delta function. Note that the moment C_{Mo} has been defined positive when counterclockwise.

The output force and moment can be modeled in general as

$$C_{Lo} = k_{h0} + k_h \dot{h} + b_h \dot{h}, \quad (2)$$

$$C_{Mo} = k_{\alpha 0} + k_{\alpha} \alpha + b_{\alpha} \dot{\alpha}, \quad (3)$$

where a dot denotes derivative with respect to t . Here k_{α} is the dimensionless stiffness of the torsional spring, or rotational stiffness, which will be present in all the results of the present work, both for the propulsion of a passively-pitching foil and for an energy harvester with passive-pitch flapping foil. In the last case of an energy harvesting device, we also include a linear spring of dimensionless stiffness k_h , and both linear and torsional dampers with dimensionless damping coefficients b_h and b_{α} , respectively. The additional coefficients k_{h0} and $k_{\alpha 0}$ are related to the dry friction, accounting also for equilibrium positions of the linear and torsional springs different from $h = 0$ and $\alpha = 0$, respectively. For simplicity, they will be set to zero in all the reported results. Thus, in the foil propulsion problem only k_{α} will be different from zero, while b_h and b_{α} will be relevant in the energy harvesting problem since the dampers will model the energy sinks which convert the mechanical energy associated to the heaving and pitching motions into electricity by an electric generator.

Finally, the dimensionless quantities

$$R(x) = \frac{\rho_s(x)\varepsilon(x)}{\rho c}, \quad S(x) = \frac{E(x)\varepsilon^3(x)}{\rho U^2 c^3}, \quad (4)$$

are the mass ratio and stiffness of the foil (see, e.g., Moore, 2017), respectively, where ρ_s is the foil's density, E its elastic modulus and ε its thickness. These quantities are allowed to vary along the foil's chord.

Without the terms with C_{Li} , C_{Lo} and C_{Mo} , Eq. (1) has been recently solved numerically in the present limit of linear potential flow for a general foil kinematics $z_s(x, t)$, but pivoting at the leading edge ($a = -1$), for constant stiffness S by Moore (2017) and Floryan and Rowley (2018), and for distributed flexibility by Floryan and Rowley (2020). Here we shall follow a different approach, by assuming a lowest order flexural motion of the foil and solving for the different moments of Eq. (1), thus obtaining useful analytical solutions, but limited to small flexural deflections. This approach has been recently used for the propulsion problem of a foil with prescribed heaving and pitching motion and passive flexural deflection (Fernandez-Feria and Alaminos-Quesada, 2021), without considering the energy harvesting problem (i.e., with $C_{Lo} = C_{Mo} = 0$), and without considering the beneficial effect that a passive pitching about an arbitrary pivot point may have on both propulsion and harvesting problems. In addition, to these new terms, the problem is formulated here in a more general form for any mass and stiffness distributions of the foil $R(x)$ and $S(x)$.

To that end we use the nondimensional lift and the moment exerted by the fluid on the foil, defined as

$$C_L(t) = \frac{L(t)}{\rho U^2 c/2} = \int_{-1}^1 \Delta C_p(x, t) dx, \quad (5)$$

$$C_M(t) = \frac{M(t)}{\rho U^2 c^2/2} = \frac{1}{2} \int_{-1}^1 (x - a) \Delta C_p(x, t) dx, \quad (6)$$

where L and M are the lift force and moment (with respect to the pivot $x = a$) per unit span, respectively. Note that C_M thus defined is positive when the moment is counterclockwise. Integrating equation (1) along the foil's chord, and the same equation multiplied by $x - a$, respectively, one obtains

$$2 \frac{d^2}{dt^2} \int_{-1}^1 R z_s dx + \frac{2}{3} \left[\frac{\partial}{\partial x} \left(S \frac{\partial^2 z_s}{\partial x^2} \right) \right]_{x=-1}^{x=1} = C_L + C_{Li} - C_{Lo}, \quad (7)$$

$$2 \frac{d^2}{dt^2} \int_{-1}^1 (x - a) R z_s dx + \frac{2}{3} \left[(x - a) \frac{\partial}{\partial x} \left(S \frac{\partial^2 z_s}{\partial x^2} \right) - S \frac{\partial^2 z_s}{\partial x^2} \right]_{x=-1}^{x=1} = 2(C_M + C_{Mo}), \quad (8)$$

where the stiffness terms have been integrated by parts. Though C_M and C_{M_0} are defined both positive when counter-clockwise, they obviously may have different signs when computed with (3) and (6), respectively.

The next moment of the Euler–Bernoulli equation is also needed in the present approach, i.e., the integral of Eq. (1) multiplied by $(x - a)^2$, which will be related to the foil’s flexural motion:

$$2 \frac{d^2}{dt^2} \int_{-1}^1 (x - a)^2 R z_s dx + \frac{2}{3} \left[(x - a)^2 \frac{\partial}{\partial x} \left(S \frac{\partial^2 z_s}{\partial x^2} \right) - 2(x - a) S \frac{\partial^2 z_s}{\partial x^2} + 2S \frac{\partial z_s}{\partial x} \right]_{x=-1}^{x=1} - \frac{4}{3} \int_{-1}^1 \frac{\partial S}{\partial x} \frac{\partial z_s}{\partial x} dx = C_F, \tag{9}$$

where

$$C_F = \int_{-1}^1 (x - a)^2 \Delta C_p(x, t) dx \tag{10}$$

may be termed the flexural coefficient with respect to the pivot point $x = a$. Note that no simplifying assumptions about $S(x)$ or $R(x)$ have been made so far. It must be noted that Eqs. (7)–(9) are valid for $-1 < a < 1$ since the point about which the delta function is centered must be inside of the domain of integration. Thus, results given below where $a = -1$ or $a = 1$ are in fact for $a = -1 + \epsilon$ or $a = 1 - \epsilon$, respectively, with $\epsilon \ll 1$.

The coefficients C_L , C_M and C_F may be derived for a given harmonic kinematics of the foil using the vortex impulse theory within the linear potential flow limit (Fernandez-Feria, 2016; Alaminos-Quesada and Fernandez-Feria, 2020). Following (Fernandez-Feria and Alaminos-Quesada, 2021) we shall use a quartic polynomial approach for $z_s(x, t)$, which constitutes a minimal model of the flexible foil since for a lower polynomial approach the stiffness term in Eq. (1) vanishes, and, consequently, all the corresponding terms in the moment Eqs. (7)–(9), so that these equations cannot relate the (unknown) flexural deflection $d(t)$, defined below, with the stiffness S , if S is constant. Thus, to the displacement of the foil as a rigid beam, $z_s = h(t) - (x - a)\alpha(t)$, describing the heaving and pitching motion about $x = a$ (in the present case the heaving $h(t)$ is given and the pitching $\alpha(t)$ unknown), we add three more terms proportional to $(x - a)^n$, $n = 2, 3$ and 4 , describing the (unknown) flexural deflection $d(t)$, also about the pivot $x = a$, which are related to each other by the boundary conditions of a free trailing edge, namely $\partial^2 z_s / \partial x^2 = \partial^3 z_s / \partial x^3 = 0$ at $x = 1$. This yields

$$z_s(x, t) = h(t) - (x - a)\alpha(t) + (x - a)^2 d(t) - (x - a)^3 \frac{2d(t)}{3(1 - a)} + (x - a)^4 \frac{d(t)}{6(1 - a)^2}. \tag{11}$$

The flexural deflection amplitude $|d|$, like $|h|$ and $|\alpha|$, is assumed small in the present linear theory, which would be a valid approximation for sufficiently large stiffness S of the foil. As we shall see, with this foil’s kinematics the first natural frequency of the fluid–structure system is recovered with great precision *analytically*.

It should be noticed that one could have selected a free leading edge, instead of a free trailing edge, as the additional two boundary condition, but that would not allow for a pivot point at, or close to, the leading edge, which, as we shall see, is usually an optimal choice for the propulsion, or the energy harvesting, performance of the foil. Another possibility would be to select free-end conditions at both the leading and the trailing edges, but this would require six degrees of freedom, i.e., a sixth-order polynomial in the present case, ceasing to be a minimal model for the flexible foil (see Anevlavi et al., 2020, for a similar problem using six Hermite shape functions).

With this approximation, Eqs. (7)–(9) can be written, for constant S but allowing for arbitrary mass distribution $R(x)$, as

$$m [\ddot{h} + (a - x_0)\ddot{\alpha}] + J_a \ddot{d} + \frac{16}{3(1 - a)^2} S d = C_L + C_{L_i} - C_{L_o}, \tag{12}$$

$$m(x_0 - a)\ddot{h} - I_a \ddot{\alpha} + J_a \ddot{d} - \frac{16a}{3(1 - a)^2} S d = 2(C_M + C_{M_0}), \tag{13}$$

$$I_a \ddot{h} - I_a \ddot{\alpha} + K_d \ddot{d} + \frac{16}{3} \frac{a^2 + \frac{1}{3}}{(1 - a)^2} S d = C_F. \tag{14}$$

Note that, contrary to the torques, the sign of α has been defined positive in (11) when clockwise, to follow the usual convention in aerodynamics. In these expressions, x_0 is the location of the foil’s center of mass, and the dimensionless mass m , the dimensionless moment of inertia about $x = a$, I_a , and all the other dimensionless moments about the pivot point, are defined as follows:

$$m = 2 \int_{-1}^1 R dx = 4R, \tag{15}$$

$$m(x_0 - a) = 2 \int_{-1}^1 (x - a)R dx = -4aR, \quad x_0 = 2 \int_{-1}^1 xR dx \tag{16}$$

$$I_a = 2 \int_{-1}^1 (x-a)^2 R dx = 4R \left(\frac{1}{3} + a^2 \right), \quad (17)$$

$$J_a = 2 \int_{-1}^1 \left[(x-a)^2 - \frac{2(x-a)^3}{3(1-a)} + \frac{(x-a)^4}{6(1-a)^2} \right] R dx = 2R \left[a^2 - \frac{2}{3}a - \frac{1}{3} + \frac{16}{15(1-a)^2} \right], \quad (18)$$

$$I_d = 2 \int_{-1}^1 (x-a)^3 R dx = -4Ra(1+a^2), \quad (19)$$

$$J_d = 2 \int_{-1}^1 \left[(x-a)^3 - \frac{2(x-a)^4}{3(1-a)} + \frac{(x-a)^5}{6(1-a)^2} \right] R dx = 2R \frac{-12 - 93a + 60a^2 - 110a^3 + 120a^4 - 45a^5}{45(1-a)^2}, \quad (20)$$

$$K_d = 2 \int_{-1}^1 \left[(x-a)^4 - \frac{2(x-a)^5}{3(1-a)} + \frac{(x-a)^6}{6(1-a)^2} \right] R dx \\ = 2R \frac{141 + 168a + 1281a^2 - 1120a^3 + 1015a^4 - 840a^5 + 315a^6}{315(1-a)^2}, \quad (21)$$

where the expressions on the right-hand sides correspond to constant R , i.e., when the center of mass coincides with the center of the foil, $x_0 = 0$. In the limit of a rigid foil ($S \rightarrow \infty$), the flexural equation (14) correctly yields that the deflection vanishes as $|d| \sim S^{-1}$. However, this means that the terms containing S in the Eqs. (12) and (13) do not vanish in this limit, so that the rigid foil equations for the vertical force and the moment about the pivot axis are not correctly recovered. But this is an artifact of the present approximation, where the displacement (11) is truncated as a quartic polynomial. It can be fixed by using a higher polynomial approximation, selecting the coefficients so that these terms vanish, while retaining the corresponding term in (14). However, this would complicate unnecessarily the present approximation, that minimally accounts for the stiffness effect within the Euler–Bernoulli beam equation, because the resulting expressions for C_L , C_M , C_F (and, especially, for the thrust coefficient C_T considered below) would become cumbersome. Thus we adopt the simplest approach with Eqs. (12) and (13) without the S -terms, and Eq. (14) with that term from the present quartic approximation, as a lowest order model that takes into account the flexibility effect on a foil with forced heave and with passive pitching and flexural deflection motions, valid for sufficiently large stiffness S and for frequencies below the second natural frequency of the system. As we shall see, this approach reproduces accurately the first natural frequency of the system and previous numerical results for the propulsion force obtained from a more general small-amplitude inviscid theory (Moore, 2015). These comparisons will thus constitute a validation of the present formulation.

Since C_L , C_M and C_F can be computed in terms of $h(t)$, $\alpha(t)$ and $d(t)$ (analytically in the case of a harmonic motion of the foil, see below), Eqs. (12)–(14) can be solved for the passive pitching and flexural motions, $\alpha(t)$ and $d(t)$, and the corresponding input forcing $C_{Li}(t)$, given $h(t)$ and the parameters in the output lift and moment, C_{Lo} and C_{Mo} .

We shall assume a harmonic motion of the foil:

$$h(t) = \Re [h_0 e^{ikt}], \quad \alpha(t) = \Re [\alpha_0 e^{ikt}], \quad d(t) = \Re [d_0 e^{ikt}], \quad (22)$$

where

$$k = \frac{\omega C}{2U} \quad (23)$$

is the reduced frequency and \Re means real part. For simplicity sake, it is assumed that h_0 is real and

$$\alpha_0 = a_0 e^{i\phi}, \quad d_0 = d_m e^{i\psi}, \quad (24)$$

with ϕ the phase shift between the heaving and pitching motions of the foil, ψ the phase shift between the heaving and deflection motions, a_0 the maximum pitch amplitude at $x = a$, and d_m the amplitude of the flexure component of the motion. In what follows we shall work with the complex expressions knowing that we have to take the real part of the results.

For this harmonic motion of the foil, the coefficients C_L , C_M and C_F are given analytically in Fernandez-Feria and Alaminos-Quesada (2021) in terms of h , α and d , thus closing the system of Eqs. (12)–(14). These expressions are given in Appendix A for easy reference, but in a more convenient form, in terms of $h(t)$, $\alpha(t)$ and $d(t)$ explicitly.

3. Analytical expressions for the pitching and deflections motions, and for the propulsive/energy harvesting performance

Eqs. (13)–(14), together with the expressions (A.2), (A.3) and (3) for C_M , C_F and C_{Mo} , respectively, and the kinematics (22)–(24), constitute a linear system of algebraic equations for the pitch and flexural deflection amplitudes, a_0 and d_m , as well as for their respective phase shifts ϕ and ψ in relation to the imposed heaving motion. These quantities are obtained in terms of the heave amplitude h_0 , the pivot and center of mass locations, a and x_0 , the stiffness and mass ratio of the foil, S and $R(x)$, the rotational stiffness, k_α , and, in the energy harvesting problem, the remaining coefficients in (2) and (3). Once the pitch and quartic deflection have been obtained, Eq. (12), together with (A.1) for C_L and (2) for C_{Lo} , yields

the input lift C_{Li} necessary to generate the prescribed heaving motion and, therefore, to compute the input power and the corresponding efficiency of the system. When the propulsion problem is considered, one has to compute also the thrust force from the prescribed and computed displacements of the foil, and then the efficiency, which is the generated thrust power divided by the input power. In the case of the energy harvesting problem, the power output is proportional to C_{Lo} and C_{Mo} , as described below in this section.

From Eqs. (13)–(14), the solution for the pitching and flexural deflection motions is obtained from a linear system of two complex equations which can be formally written as

$$\mathbf{A} \cdot \mathbf{X} = \mathbf{b} \quad \text{with} \quad \mathbf{A} = \begin{pmatrix} A_{11} & A_{12} \\ A_{21} & A_{22} \end{pmatrix}, \quad \mathbf{X} = \begin{pmatrix} \frac{a_0 e^{i\phi}}{h_0} \\ \frac{d_m e^{i\psi}}{h_0} \end{pmatrix}, \quad \mathbf{b} = \begin{pmatrix} b_1 \\ b_2 \end{pmatrix}, \quad (25)$$

where the different coefficients A_{ij} and b_j , which are given in Appendix B, depend on all the dimensionless parameters except for h_0 , which is absorbed into the solution \mathbf{X} due to the linearity of the problem (the pitch and flexure amplitudes increase linearly with the heave amplitude).

It is useful to check first whether these equations model correctly the motion of the foil in absence of fluid–structure interaction (FSI); i.e., assuming $C_L = C_M = C_F = 0$. Considering only the case in which $C_{Mo} = k_\alpha \alpha$ (i.e., the propulsion problem with $b_\alpha = 0$), and assuming firstly a rigid foil ($S \rightarrow \infty$), the last linear equation in (25) just tells us that there is no flexural deflection ($d_m = 0$). From the first one,

$$a_0 e^{i\phi} = \frac{m(a - x_0)k^2 h_0}{2k_\alpha - I_a k^2} = \frac{2Rak^2 h_0}{k_\alpha - 2R \left(a^2 + \frac{1}{3} \right) k^2}, \quad (26)$$

so that $\phi = 0$ or $\phi = \pi$ depending on the sign of the right hand side (the right most expression is for constant R). From Eq. (12), the corresponding input lift is $C_{Li} = \Re[C_i e^{ikt}]$, with $C_i = -mk^2 h_0 [1 + m(a - x_0)^2 k^2 / (2k_\alpha - I_a k^2)]$. The vanishing denominator in (26) yields the dimensionless frequency of the first (and only one in the present approximation) resonant mode of the system, now consisting of just a rigid plate with a spring of torsional stiffness k_α at $x = a$:

$$k_{r0} = \sqrt{\frac{2k_\alpha}{I_a}} = \sqrt{\frac{k_\alpha}{2R \left(a^2 + \frac{1}{3} \right)}}, \quad (27)$$

the last expression being valid for constant mass ratio R . In terms of dimensional variables, writing the output power as $M_o = (1/2)\rho U^2 c^2 b k_\alpha \alpha \equiv K_\alpha \alpha$, where b is the span of the plate and K_α the dimensional stiffness of the torsional spring, the (dimensional) natural frequency can be written in the standard form, $\omega_{r0} = \sqrt{K_\alpha / \mathcal{I}_a}$, where \mathcal{I}_a is the moment of inertia about the pivot point, given by $\mathcal{I}_a = \rho_s \varepsilon c^3 b (1 + 3a^2) / 12$ for constant density and thickness distributions, $\rho_s \varepsilon = \text{constant}$.

Secondly, in the opposite limit of a flexible foil with finite stiffness S but with the passive pitching motion inhibited by an infinite torsional stiffness ($k_\alpha \rightarrow \infty$), the first linear equation in (25) tells us that $a_0 = 0$. From the second equation,

$$d_m e^{i\psi} = \frac{I_a k^2 h_0}{\frac{16(a^2 + 1/3)}{3(1 - a)^2} S - K_d k^2}. \quad (28)$$

The corresponding (first) resonant frequency is

$$k_{r0} = \sqrt{\frac{16(a^2 + 1/3)S}{3(1 - a)^2 K_d}} = \sqrt{\frac{280(1 + 3a^2)S}{(141 + 168a + 1281a^2 - 1120a^3 + 1015a^4 - 840a^5 + 315a^6)R}}, \quad (29)$$

with the last expression valid for constant mass ratio R , recovering the well known result that the dimensionless natural frequencies of a flexible plate are proportional to $\sqrt{S/R}$ (e.g., Floryan and Rowley, 2018), but now with an analytical expression for its dependence on the pivot point location in the present approximation. For a pivot at the leading edge ($a = -1$), $k_{r0} = \sqrt{35S/(142R)} \simeq 0.496 \sqrt{S/R}$, recovering almost exactly the result from a more general theory by Floryan and Rowley (2018) in the limit $R \gg 1$, when the FSI is negligible.

Finally, for a flexible plate with quartic deflection and passive pitching, but still without considering FSI (and with $C_{Mo} = k_\alpha \alpha$), the dimensionless, first natural frequency of the system can be obtained from $\det(\mathbf{A}) = 0$. It is given by the positive root of

$$k_{r0}^2 = \frac{1}{9(1 - a)^2(I_d J_d - I_a K_d)} \left\{ -8(3a^2 + 1)I_a S - 9(1 - a)^2 K_d k_\alpha + \left[288(3a^2 + 1)(1 - a)^2(I_d J_d - I_a K_d)k_\alpha S + [9(1 - a)^2 K_d k_\alpha + 8I_a(1 + 3a^2)S]^2 \right]^{1/2} \right\}. \quad (30)$$

Returning now to the problem with FSI, i.e., considering the effect of C_M and C_F in solving (25), the matrix \mathbf{A} is no longer real as in the last cases considered, even for a rigid foil, and there is no proper resonant frequency at which a_0 and/or d_m become singular. But there exists a frequency that maximizes the pitch amplitude, and therefore the thrust force (see Section 4 below), for each set of dimensionless parameters. Since at this frequency, $k = k_r$ say, which corresponds to the minimum value of $|\det(\mathbf{A})|$, the maximum of a_0 and/or d_m are quite large, it may still be called the resonant frequency, as in Moore (2014). Obviously, this frequency tends to the resonant frequency k_{r0} described above for $R \rightarrow \infty$, as the FSI become negligible.

Once the linear system (25) is solved for \mathbf{X} , the modulus of each one of its two components yields the relative pitch and quadratic deflection amplitudes, a_0/h_0 and d_m/h_0 , respectively, and their arguments provide the phase shifts ϕ and ψ . Then, Eq. (12) yields the required input lift C_{Li} , and hence the input power coefficient:

$$C_{Pi}(t) = \dot{h}(t)C_{Li}(t). \quad (31)$$

Note from Eq. (12) that this expression coincides with the usual one $C_{Pi} = -\dot{h}(t)C_L(t)$ for the propulsion of a heaving foil only for very small mass ratios ($R \rightarrow 0$), provided that $C_{Lo} = 0$ (propulsion problem).

For the **propulsion problem** ($b_\alpha = 0$), one has to obtain the propulsion coefficient $C_T(t)$ from the resulting pitching and flexural deflection motions, $\alpha(t)$ and $d(t)$, respectively, and the given heaving kinematics $h(t)$. In the case of a quadratic deflection, i.e., with z_s given by (11) without the cubic and quartic terms, $C_T(t)$ is given by Eq. (4.5) in Alaminos-Quesada and Fernandez-Feria (2020). For the quartic deflection (11) the thrust coefficient is derived in a similar way, containing some additional terms. The propulsive (Froude) efficiency is defined as

$$\eta_p = \frac{\bar{C}_T}{\bar{C}_{Pi}}, \quad (32)$$

where the bar denotes time average over a period of the foil's harmonic motion,

$$\bar{C}_T = \frac{k}{2\pi} \int_t^{t+2\pi/k} C_T(t) dt, \quad (33)$$

and similarly for \bar{C}_{Pi} .

The mean value of the thrust coefficient $C_T(t)$ for a given heaving, pitching and flexural motion can be written as

$$\begin{aligned} \bar{C}_T = (kh_0)^2 [& t_h(k) + t_{hp}(k, a, \phi)\theta + t_p(k, a)\theta^2 + t_{dh}(k, a, \psi)\theta_{dh} + \\ & + t_{pd}(k, a, \psi, \phi)\theta_{dh}\theta + t_d(k, a)\theta_{dh}^2], \end{aligned} \quad (34)$$

with the functions $t_h(k)$, $t_{hp}(k, a, \phi)$, $t_p(k, a)$, $t_{dh}(k, a, \psi)$, $t_{pd}(k, a, \phi, \psi)$ and $t_d(k, a)$ given in Appendix C. In this expression use has been made of the nondimensional parameters

$$\theta = \frac{a_0}{kh_0}, \quad \theta_{dh} = \frac{d_m}{kh_0}, \quad (35)$$

where θ is the well-known Lighthill's (1969) feathering parameter. For $\theta_{dh} = 0$ we have the mean thrust coefficient \bar{C}_T^0 of a rigid foil with the same heaving and pitching motions (Fernandez-Feria, 2016, 2017). The time-averaged input power coefficient can be written as a sum of several terms:

$$\bar{C}_{Pi} \equiv \bar{h}C_{Li} = \bar{C}_{Pi}^0 + \bar{C}_{Pi}^d + \bar{C}_{Pi}^m + \bar{C}_{Pi}^{poh}. \quad (36)$$

\bar{C}_{Pi}^0 is the FSI contribution from the terms in C_L associated to the motion of the foil as a rigid solid,

$$\bar{C}_{Pi}^0 = \pi(kh_0)^2 \left\{ \mathcal{F} - \theta \left[\left(\frac{k}{2} + \left(\frac{1}{2} - a \right) k\mathcal{F} + \mathcal{G} \right) \cos \phi + \left(\frac{a}{2}k^2 + \left(a - \frac{1}{2} \right) \mathcal{G}k + \mathcal{F} \right) \sin \phi \right] \right\}. \quad (37)$$

This obviously coincides with the contribution from C_L in Theodorsen's power coefficient for a rigid foil (Theodorsen, 1935; Garrick, 1936), where \mathcal{F} and \mathcal{G} are the real and imaginary parts of Theodorsen's function \mathcal{C} given in Eq. (A.5). The other contribution from the FSI, associated to the flexural deflection motion of the foil (i.e., from terms in C_L containing d), is

$$\bar{C}_{Pi}^d = \pi kh_0 d_m \left[\left(A_{l2} \frac{k^2}{2} - A_{g1} k\mathcal{G} + A_{g0}\mathcal{F} \right) \sin \psi + \left(-A_{l1} \frac{k}{2} + A_{g1} k\mathcal{F} + A_{g0}\mathcal{G} \right) \cos \psi \right], \quad (38)$$

where A_{l1} , A_{l2} , A_{g0} and A_{g1} are functions of a defined in Eqs. (A.6)–(A.10) in Appendix A. The term \bar{C}_{Pi}^m is the contribution from the inertia of the foil,

$$\bar{C}_{Pi}^m = -\frac{k^3 h_0}{2} [m(a - x_0)a_0 \sin \phi + J_a d_m \sin \psi]. \quad (39)$$

Finally, \bar{C}_{Poh} is the contribution from C_{Lo} , appearing only in the energy harvesting problem, termed in that way because it coincides with one of the contributions to the power output in that problem (see immediately below),

$$\bar{C}_{Poh} = b_h \frac{k^2 h_0^2}{2}. \tag{40}$$

In the case of the **energy harvesting problem**, by assuming that the loss of mechanical energy through the linear and torsional dampers is completely converted into electric energy, the dimensionless time-averaged power output is

$$\bar{C}_{Po} \equiv \bar{C}_{Poh} + \bar{C}_{Poa} = \overline{hC_{Lo}} + 2\overline{\alpha C_{Mo}} = b_h \overline{h^2} + 2b_\alpha \overline{\alpha^2} = (kh_0)^2 \left(\frac{1}{2} b_h + b_\alpha k^2 \theta^2 \right). \tag{41}$$

The system works as an energy harvester if the net power output $\bar{C}_{Po} - \bar{C}_{Pi}$ is positive. One may define the efficiency of the energy harvesting as

$$\eta_e = \frac{\bar{C}_{Po} - \bar{C}_{Pi}}{h_0 + (1 + |a|)a_0 + d_m}, \tag{42}$$

which is the usual Betz efficiency, commonly used in the turbine literature (Xiao and Zhu, 2014; Young et al., 2014), defined as the portion of the incoming flow kinematic energy flux (i.e., $\rho U^3 b \Delta / 2$) extracted by the system, where $\Delta = (h_0 + (1 + |a|)a_0 + d_m)c$ is the largest possible total distance swept by any portion of the foil. We shall use the normalized quantity

$$\hat{\eta}_e = \frac{\eta_e}{h_0}, \tag{43}$$

which is independent of the heave amplitude h_0 in the present linear theory for small amplitude, but which is not an efficiency properly because it could be larger than unity.

4. Results

4.1. Propulsion of a heaving rigid foil with passive pitching

First, the propulsion problem ($C_{Lo} = 0$ and $b_\alpha = 0$) of a rigid foil ($S \rightarrow \infty$) with uniform mass distribution R ($x_0 = 0$) pivoting about an arbitrary point $x = a$ is considered, which is the same problem analyzed by Moore (2014) when the pivot is at the leading edge ($a = -1$). Eq. (14) is not needed and Eq. (25) reduces to

$$A_{11} \frac{a_0}{h_0} e^{i\phi} = b_1, \tag{44}$$

so that

$$\frac{a_0}{h_0} = \left| \frac{b_1}{A_{11}} \right| \quad \text{and} \quad \phi = \arg \left(\frac{b_1}{A_{11}} \right). \tag{45}$$

When the FSI is neglected, $|A_{11}|$ vanishes at the first resonant frequency (27), and the pitch amplitude a_0 becomes singular. Now, when the FSI is considered, no proper resonant frequency at which a_0 becomes singular does exist, but there is a frequency k_r that maximizes the pitch amplitude which, as aforementioned, will still be called the resonant or natural frequency. As shown in Fig. 2, where k_r and k_{r0} from (27) are plotted vs. R for two values of k_α , this resonant frequency coincides with that of Moore (2014), which is included in Fig. 2 in its simplest approximation valid for large k_α and $a = -1$ (Eq. (3.4) in Moore (2014)). For large R , k_r obviously tends to k_{r0} since the FSI becomes irrelevant, the more so the larger k_α . However, for small R the natural frequency k_r may become quite different from its quiescent counterpart k_{r0} , specially as k_α decreases.

These resonant frequencies are basically those at which there is a marked enhancement of both thrust and power in relation to their values for a purely heaving motion of the foil, \bar{C}_T / \bar{C}_T^0 and $\bar{C}_{Pi} / \bar{C}_{Pi}^0$, respectively, as shown in Fig. 3 for a foil of negligible inertia ($R = 0$) pivoting at the leading edge ($a = -1$) for several spring stiffness k_α . Obviously, the results for a purely heaving motion coincide with the present ones for a clamped leading edge ($k_\alpha \rightarrow \infty$). This figure is basically the same as Fig. 3 in Moore (2014), but representing the relative thrust and power coefficients, and the relative efficiency $\eta_p - \eta_p^0$, instead of their absolute values. Note that the dimensionless spring stiffness K in Moore (2014) is the present $k_\alpha / 2$. Fig. 3 indicates that maximum efficiency enhancement does not correspond with maximum thrust enhancement, the last happening at the resonant frequencies for given k_α . In fact, the maximum gain in efficiency is achieved for vanishing spring stiffness at the leading edge, a result previously reported by several authors in the present inviscid limit (Moore, 2014, 2015; Floryan and Rowley, 2020). It is remarkable that the present results are basically the same as those obtained by Moore (2014) for $a = -1$ in spite of the quite different approaches, both for the FSI formulations and, specially, for the computation of the thrust, which here is obtained from a vortex impulse theory (Fernandez-Feria, 2016).

To check the present results for other pivot locations and against experimental data, Fig. 4 compares results from the present model with experimental measurements by Asselin and Williamson (2019) of the resulting pitching amplitude

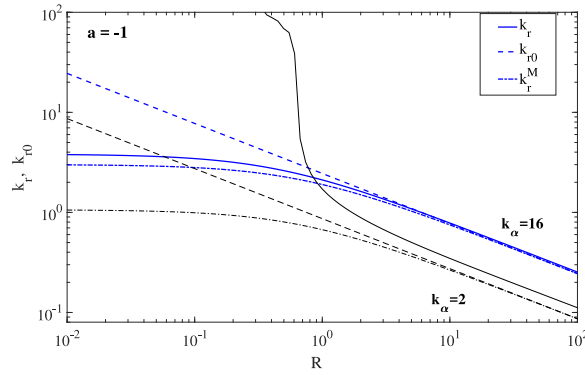


Fig. 2. Resonant frequencies k_r (solid lines) and k_{r0} given by (27) (dashed lines) vs. R for $a = -1$ and two values of k_α , as indicated. k_r^M (dashed-and-dotted lines) is the approximation for the resonant frequency obtained by Moore (2014) (his equation (3.4)) valid for large k_α and $a = -1$.

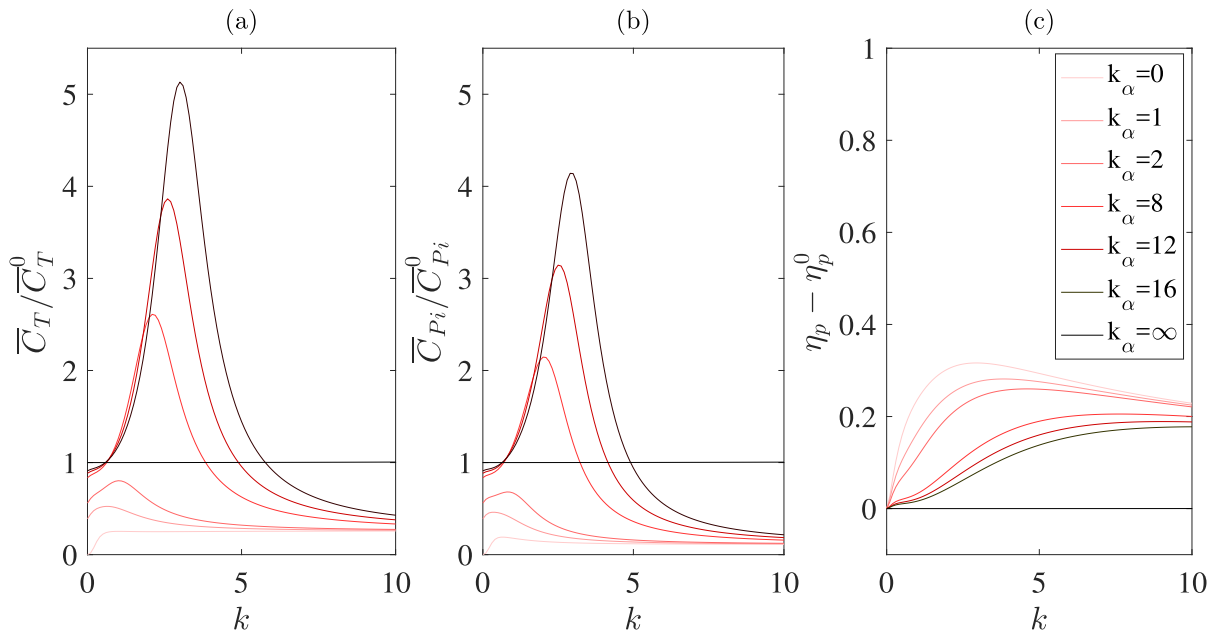


Fig. 3. Ratios of the time-averaged thrust (a) and power (b) coefficients to the mean thrust and power coefficients of an otherwise identical foil with heaving-only motion, \bar{C}_T/\bar{C}_T^0 and $\bar{C}_{Pi}/\bar{C}_{Pi}^0$, respectively, as a function of the reduced frequency for increasing values of the spring stiffness k_α . (c): Relative efficiency to the heaving-only motion, $\eta_p - \eta_p^0$, vs. k for the same cases. $R = 0$ and $a = -1$ in all cases.

and thrust coefficient of a heaving airfoil with passive pitching in their cyber-physical fluid dynamics experimental setup. These authors fix the frequency k and the heaving amplitude h_0 and vary the spring stiffness k_α , representing their results in terms of the relative frequency f/f_n , where f_n is the natural frequency (27) (i.e., neglecting FSI). In the present notation, $f/f_n = k/\sqrt{k_\alpha/[2R(a^2 + 1/3)]}$, where k is fixed to $\pi/2$ and k_α is varied. No value of the mass ratio R is provided. Since the experiments are in water but with a relatively thick airfoil (NACA0012), it should be small, but not too much. We adjust R by fitting the maximum pitch amplitude in their experiments for several pivot positions, even far upstream of the leading edge ($a < -1$ in the present notation; Fig. 4(a)), resulting $R \simeq 0.85$. With this value of R all the maxima of the pitch amplitude are well captured, though the corresponding resonant frequencies are under-predicted. In Fig. 4(b) we compare the resulting thrust coefficient with the experimental data. In spite of the fact that the flapping amplitudes in the experiments are not small ($h_0 = 0.5$ and some of the resulting amplitudes a_0 shown in Fig. 4(a) are larger than 45°), the present linear theory captures reasonably well the main features of the dynamics of the flapping airfoil.

To finish this subsection, some more exhaustive results for the thrust coefficient and the propulsive efficiency are presented in Figs. 5 and 6 as contour plots in both the frequency-spring stiffness and the frequency-pivot point planes. Fig. 5 shows that, as aforementioned, propulsive enhancement by passive pitching is generated around the natural frequencies of the system when the pivot point is at the leading edge, provided that the torsional spring is stiff enough

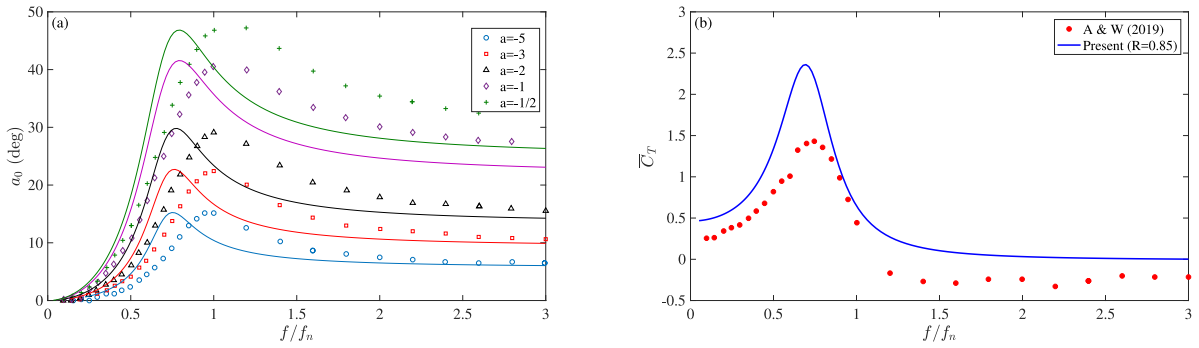


Fig. 4. Comparison with experimental measurements by Asselin and Williamson (2019) (symbols) with the present theoretical results (lines) for the pitch amplitude (a) and the thrust coefficient (b) vs. the frequency relative to the natural quiescent frequency of the system. The experiments are made with a NACA0012 airfoil at Reynolds number 10^4 , with $h_0 = 0.5$, $k = \pi/2$, several values of a and varying k_α . $a = -1$ in (b), and $R = 0.85$ in all the theoretical results (see main text).

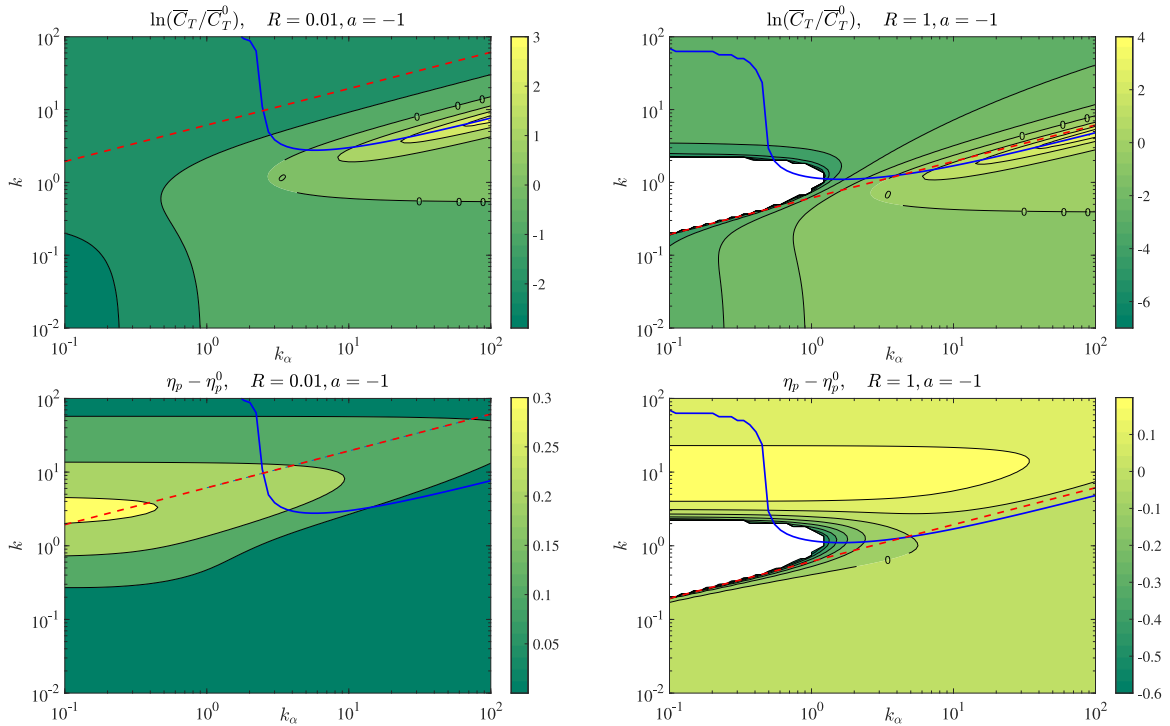


Fig. 5. Relative thrust coefficient (top panels) and efficiency (bottom panels) as a function of frequency k and spring stiffness k_α for forced heaving motion with passive pitching at the leading ($a = -1$) of a rigid foil for two mass ratios, $R = 0.01$ (left panels) and $R = 1$ (right panels). Lines marked with ‘0’ indicate where the passively pitching foil has the same thrust, or efficiency, as the equivalent heaving-only foil with $k_\alpha \rightarrow \infty$ (\bar{C}_T^0 and η_p^0 , respectively). Areas with negative thrust have been whited out. The thick continuous lines correspond to the first natural frequency of the system (maximum pitch amplitude), while the dashed lines represent this frequency without FSI (Eq. (27)).

(large k_α). The predicted increase in thrust can be very large, but restricted to a narrow region in the $k_\alpha - k$ plane (top panels in Fig. 5). On the other hand, efficiency enhancement is obtained for practically any value of k and k_α plotted in Fig. 5 (bottom panels), but it is relatively weak and with the maximum values located in the opposite limit of low stiffness, without connection to the natural frequency of the system. Thus, with this flapping system activated at the leading edge it seems more interesting to work with a stiff spring in the thrust enhancement region close to the resonant frequencies of the system, as already noted in previous works (Moore, 2014, 2015; Asselin and Williamson, 2019). The effect of the mass ratio R is relatively small.

When the pivot point is moved (Fig. 6), the response is quite different depending on the stiffness of the torsional spring, mostly due to the different behavior of the natural frequencies, also plotted in Fig. 6 for the thrust (top panels) when $k_\alpha = 0.1$ and $k_\alpha = 10$. For low k_α , the maximum thrust enhancement is obtained when pivoting just downstream

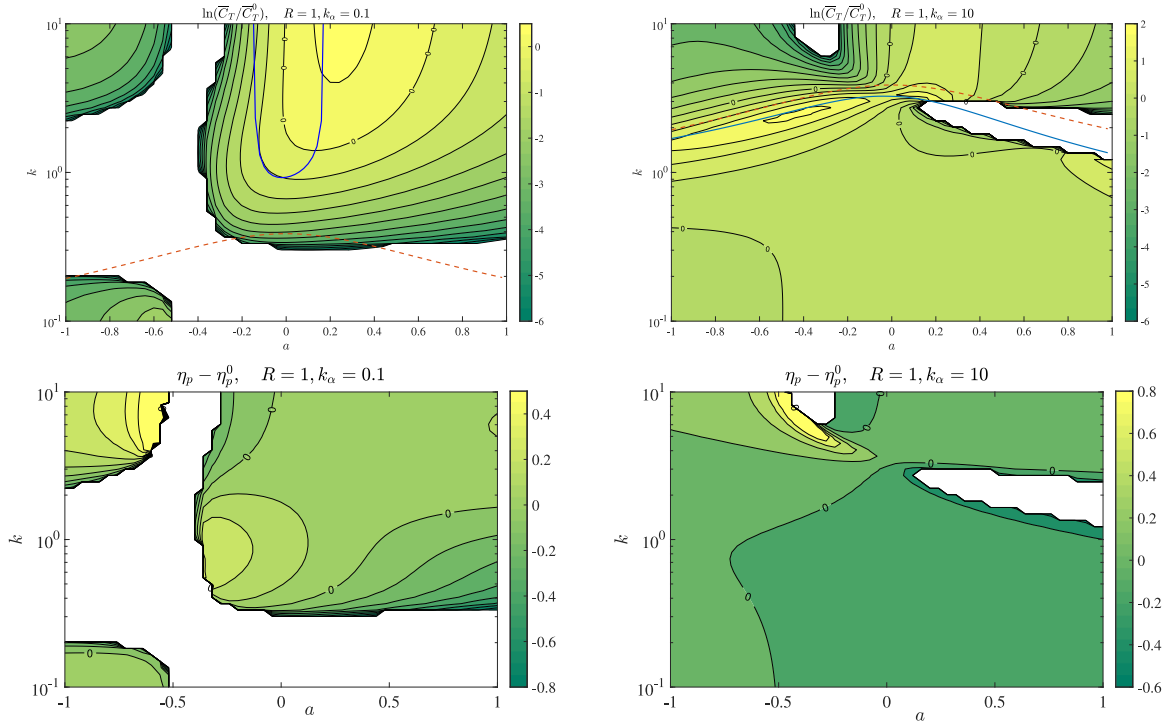


Fig. 6. Analogous to Fig. 5 but in the frequency–pivot plane for $R = 1$ and two values of the spring stiffness, $k_\alpha = 0.1$ (left panels) and $k_\alpha = 10$ (right panels).

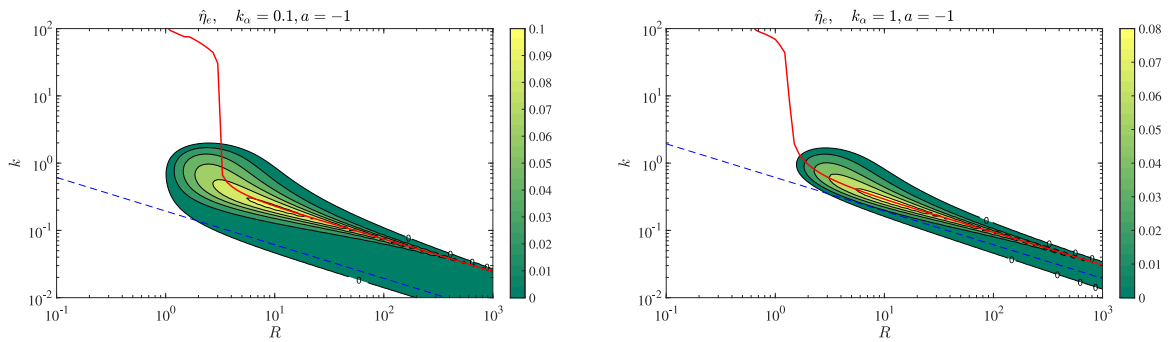


Fig. 7. Energy harvesting efficiency $\hat{\eta}_e$ as a function of frequency k and mass ratio R for forced heaving motion with passive pitching at the leading ($a = -1$) of a rigid foil for two spring stiffness, $k_\alpha = 0.1$ (left) and $k_\alpha = 1$ (right). $b_\alpha = 1$ and $b_h = 0$. The thick continuous lines correspond to the first natural frequency of the system k_r (maximum pitch amplitude), while the dashed lines represent this frequency without FSI and $b_\alpha = 0$ (i.e., Eq. (27)).

of the mid-chord point and for relatively high frequencies. The maximum efficiency enhancement, however, is obtained when pivoting near the quarter-chord point ($a = -1/2$), also for high frequencies, but with no thrust gain and in the verge of negative thrust, which means that this configuration might not be useful in practice due to the effect of friction, no considered here. There is another local maximum of efficiency at lower frequencies when a is closer to zero which may be more interesting due to the thrust enhancement. For large spring stiffness (right panels in Fig. 6 with $k_\alpha = 10$), the high thrust enhancement region is again concentrated around the natural frequencies of the system, with a maximum slightly downstream of the quarter-chord point. The maximum efficiency gain is also close to this pivot point, but for frequencies higher than the resonant one. In the case of $k_\alpha = 10$ (right panel in Fig. 6) the propulsive efficiency enhancement can be quite high, but again close to the edge of negative thrust, so that it would be wiser to work at lower frequency with larger thrust enhancement but less efficiency gain.

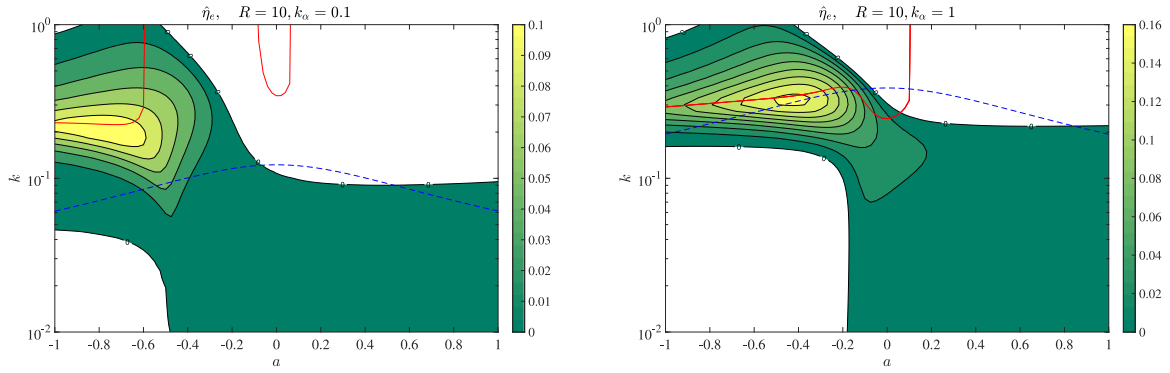


Fig. 8. Energy harvesting efficiency $\hat{\eta}_e$ as a function of frequency k and pivot point a for forced heaving motion with passive pitching of a rigid foil with mass ratio $R = 10$ for two spring stiffness, $k_{\alpha} = 0.1$ (left) and $k_{\alpha} = 1$ (right). $b_{\alpha} = 1$ and $b_h = 0$. The thick continuous lines correspond to the first natural frequency of the system k_r (maximum pitch amplitude), while the dashed lines represent this frequency without FSI and $b_{\alpha} = 0$ (Eq. (27)).

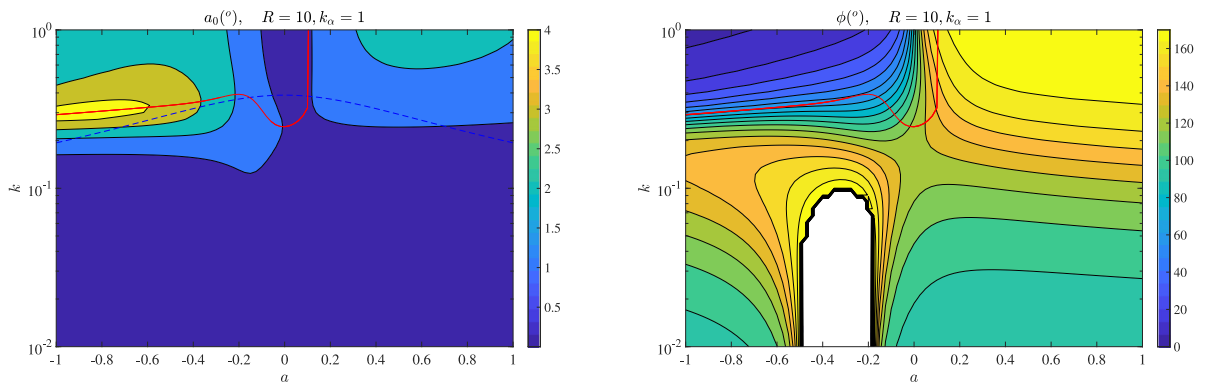


Fig. 9. Pitch amplitude a_0 (left) and phase shift ϕ (right), both in degrees, corresponding to the case plotted in Fig. 8 for $k_{\alpha} = 1$ (left).

4.2. Energy harvesting from a heaving rigid foil with passive pitching

To see the effect of passive pitch on the energy harvested by a flapping rigid foil ($S \rightarrow \infty$) we consider the case in which the energy is harvested by the torsional damper only ($b_h = 0$), normalizing the results by setting $b_{\alpha} = 1$, and assuming also that the mass ratio R is uniform ($x_0 = 0$). Fig. 7 shows contour plots of the efficiency of energy harvesting $\hat{\eta}_e$ defined in (42)–(43) in the frequency–mass ratio plane when pivoting at the leading edge ($a = -1$) for two values of the spring stiffness k_{α} . Clearly, $\hat{\eta}_e > 0$ only in a relatively narrow band around the first resonance frequency of the system $k_r(R)$, also shown in the figure, with the maximum of efficiency for each R practically coinciding with k_r . Thus, net energy can only be harvested from a current when the frequency is such that the pitch amplitude is near its maximum at $k = k_r$, provided that the mass ratio R is above a certain threshold value that depends on the spring stiffness k_{α} , which, in turn, cannot be too large (no region with positive $\hat{\eta}_e$ is found in the plane of Fig. 7 when k_{α} is larger than about 8). It is also observed in Fig. 7 that the resonant frequency $k_{r,0}$ without considering FSI, given by Eq. (27), is roughly a good lower frequency bound above which energy can be extracted from the current for given R , k_{α} and a . The natural frequency k_r is always larger than $k_{r,0}$ and it is also proportional to $R^{-1/2}$, approximately, in the region of interest with $\hat{\eta}_e > 0$.

The effect of the pivot point is shown in Fig. 8, where contours of the efficiency are plotted in the frequency–pivot plane for a mass ratio $R = 10$, which approximately corresponds to the maximum efficiency shown in Fig. 7, and the same values of the torsional spring stiffness of Fig. 7. Although $\hat{\eta}_e$ can be positive for all values of a in a low frequency region, the efficiency is only appreciable in a narrow band around the resonant frequency of the system (also shown in the figure) when it lies in this low frequency region; that is for pivots upstream of, and around of, the quarter-chord point, depending on the spring stiffness. For $k_{\alpha} = 1$, the maximum efficiency is reached when pivoting at about $a = -0.45$, i.e., close to the quarter-chord point, with a reduced frequency $k \approx 1/3$.

Fig. 9 shows the pitch angle and phase shift corresponding to this last case. The maximum pitch angle at the resonant frequency is $a_0 \simeq 4^\circ$, well within the low amplitude range of the present theory, with a phase shift $\phi \simeq 90^\circ$. These results are in qualitative agreement with (Boudreau et al., 2019b,a), who analyzed numerically the performance of free-pitching flapping-foil turbines with prescribed heave at a Reynolds number of 3.9×10^6 , but for high amplitude oscillations

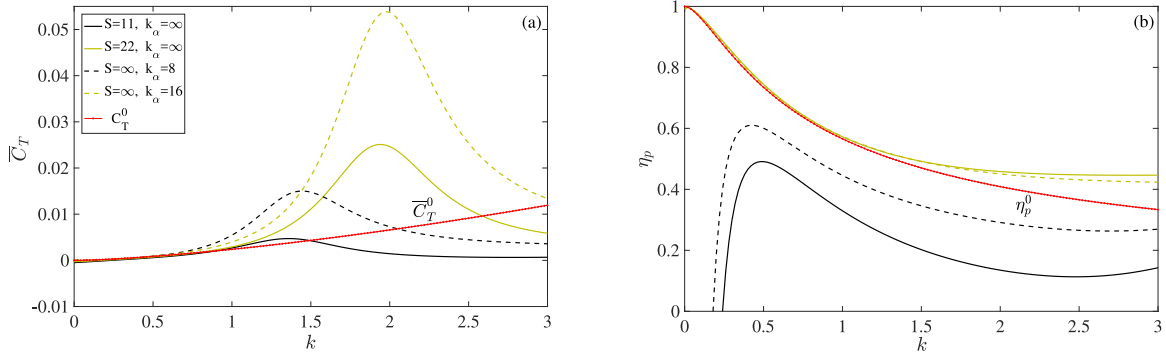


Fig. 10. Time-averaged thrust coefficient (a) and efficiency (b), compared with their values for an otherwise identical rigid foil with heaving-only motion, \bar{C}_T^0 and η_p^0 , respectively, as a function of the reduced frequency for several values of S and the spring stiffness k_α . $R = 1$ and $a = -1$.

($h_0 = 2$ and pitch amplitudes reaching values up to almost 90°) for which the present linear potential flow results are not quantitatively valid. These authors found that maximum efficiency is obtained when the pitch axis is located around the quarter-chord point, for a phase lag ϕ near 90° , provided that the moment of inertia is sufficiently large, which in the present notation means large R , according to (17), all this in good agreement with the present theoretical results. Further, they found that this maximum efficiency is reached when the moment of inertia and the pitch stiffness are scaled keeping constant a certain parameter related to the difference between the frequency and the quiescent natural frequency (27) (dashed lines in Figs. 7), which here runs almost parallel to the natural frequency obtained when FSI and b_α are taken into account (continuous lines in Figs. 7), around which the present efficiency is the highest. This explains also the result by these authors that the efficiency quickly deteriorates as the dimensionless moment of inertia and pitch stiffness are such that the pitch quiescent natural frequency k_{r0} (Eq. (27)) remains constant, which, as aforementioned, approximately marks the lower frequency limit for energy extraction in the present results. On the other hand, the constant value of their parameter ‘pitch stiffness’, where efficiency is a maximum, must roughly coincide with the present natural frequency of the system k_r , which here is obtained analytically as a function of R , k_α and the kinematic parameters.

4.3. Propulsion of a heaving foil with passive pitching and chordwise flexibility

When chordwise flexibility is allowed, both Eqs. (13) and (14) are needed to obtain simultaneously the pitch and flexural deflection amplitudes and phases, which from (25) can be written as

$$\mathbf{x} = \begin{pmatrix} \frac{a_0 e^{i\phi}}{h_0} \\ \frac{d_m e^{i\psi}}{h_0} \end{pmatrix} = \mathbf{A}^{-1} \cdot \mathbf{b}. \tag{46}$$

Fig. 10 shows some results for the thrust \bar{C}_T and the propulsive efficiency η_p , compared with their respective values for an otherwise identical rigid foil with heaving-only motion ($S = \infty$ and $k_\alpha = \infty$), \bar{C}_T^0 and η_p^0 , for several cases corresponding to Fig. 2 in Moore (2015). As this author demonstrates, a rigid foil with passive pitching about its leading edge and appropriate torsional spring constant k_α (K in Moore (2015) is the present $k_\alpha/2$) may generate substantially more thrust at a given frequency than any flexible foil for any constant value S . This is illustrated in Fig. 10, where the flexible foils with two different values of stiffness S but without passive pitching amplify less the thrust at their corresponding resonant frequencies than the rigid foils with torsional springs at their leading edges with different spring stiffness k_α , which are selected to match the resonant torsional frequencies of the flexible foils. However, the efficiency enhancement is negligible at these resonant frequencies, as already noted by Asselin and Williamson (2019) for rigid foils with passive pitching. In the case of flexible foils, the thrust amplification at the natural frequencies is not accompanied by an efficiency enhancement at all ($\eta_p < \eta_p^0$). It is remarkable that the present approximation recovers the resonant frequencies obtained numerically in Moore (2015) almost exactly, and the thrust amplification with a fairly good approximation, in spite of the quite different formulations.

To see more clearly what happens as S or k_α are varied, when a and R are fixed, Fig. 11 shows the contours of thrust and efficiency enhancement in the $S-k$ and $k_\alpha-k$ planes for given values of k_α and S , respectively. In both representations the thrust magnification is achieved around the first resonant frequency of the system $k = k_r$ that minimizes $|\det(\mathbf{A})|$ for sufficiently large S . In fact, it is the natural frequency associated to the spring stiffness k_α , or torsional spring mode, as it is close to that given by (27) when FSI is neglected, also plotted in Fig. 11 with dashed-and-dotted lines. The first natural frequency associated to the foil stiffness S , or bending mode, is not plotted since it is much higher, as indicated by its value

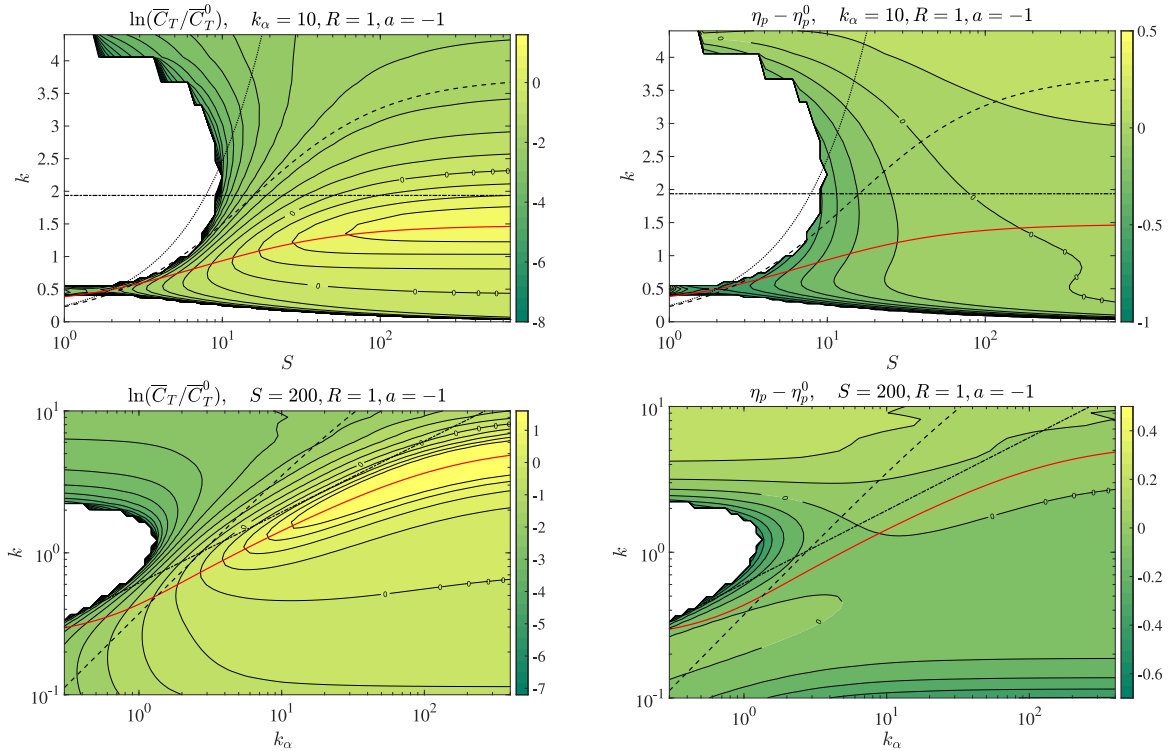


Fig. 11. Contours of thrust (left panels) and efficiency (right panels) enhancement in the (S, k) plane (top) and in the (k_α, k) plane (bottom) for $R = 1$ and $a = -1$. Lines marked with ‘o’ indicate where the passively pitching and flexible foil has the same thrust, or efficiency, as the heaving-only rigid foil counterpart. Areas with negative thrust and negative power input (for the efficiency) have been whitened out. The continuous red lines correspond to the natural frequency of the system minimizing $|\det(\mathbf{A})|$, the dashed-and-dotted lines to (27), the dashed lines to (30) and the dotted lines to (29).

when the FSI is neglected, given by (30) and plotted with dotted lines in the figure. This bending mode is also recovered by another local minimum of $|\det(\mathbf{A})|$, but it is not relevant in the present approximation since its first natural frequency is higher than the second natural frequency associated to the torsional spring mode, at which the present theory is not longer valid.

Clearly, the highest thrust enhancement is obtained along the lower frequency resonant mode associated to the torsional spring, which also depends on the flexibility of the foil when the FSI is taken into account. As shown by Moore (2015), for given spring stiffness k_α it yields the maximum thrust amplification for a rigid foil ($S \rightarrow \infty$). The corresponding optimal frequency is always lower than the resonant frequency k_{r0} given by Eq. (27), and plotted in Fig. 11 with dashed-and-dotted lines, as also noted by this author (in other words, the optimal spring stiffness is always larger than that given by Eq. (27) for an operating reduced frequency). As also shown in Fig. 11, efficiency enhancement is also achieved when operating at this torsional spring mode if the stiffness S is large enough. However, the efficiency gain is relatively small and not optimal at the maximum thrust amplification.

Fig. 11 is for $R = 1$ and $a = -1$. To see how the mass ratio and the pivot point location affect to the propulsion performance, we plot in Fig. 12 the lower resonant frequency k_r corresponding to maximum thrust enhancement in the pivot point–mass ratio plane for given values of the foil and spring stiffness, namely $S = 200$ and $k_\alpha = 10$. This figure also shows the corresponding values of thrust and efficiency enhancement. As noted above, maximum thrust amplification does not mean maximum efficiency enhancement. Thus, local maxima for thrust amplification are obtained for pivots just upstream of the quarter-chord point when R is about 2 and downstream of the mid-chord point for R small, while the maximum efficiency enhancement is achieved when pivoting just upstream of the mid-chord point for mass ratios lower than unity. Since there is no efficiency gain when pivoting downstream of the mid-chord point, the optimal propulsion conditions for these representative values of S and k_α are, according to the present approximation, for a foil with R of order unity pivoting just downstream of the quarter-chord point.

4.4. Energy harvesting performance of a heaving foil with passive pitching and chordwise flexibility

To analyze the effect of flexibility on the energy harvesting performance of the passive-pitching heaving-foil, we consider the case $R = 10$, which is one of the most favorable cases considered in Section 4.2 for a rigid foil (see Fig. 7), and

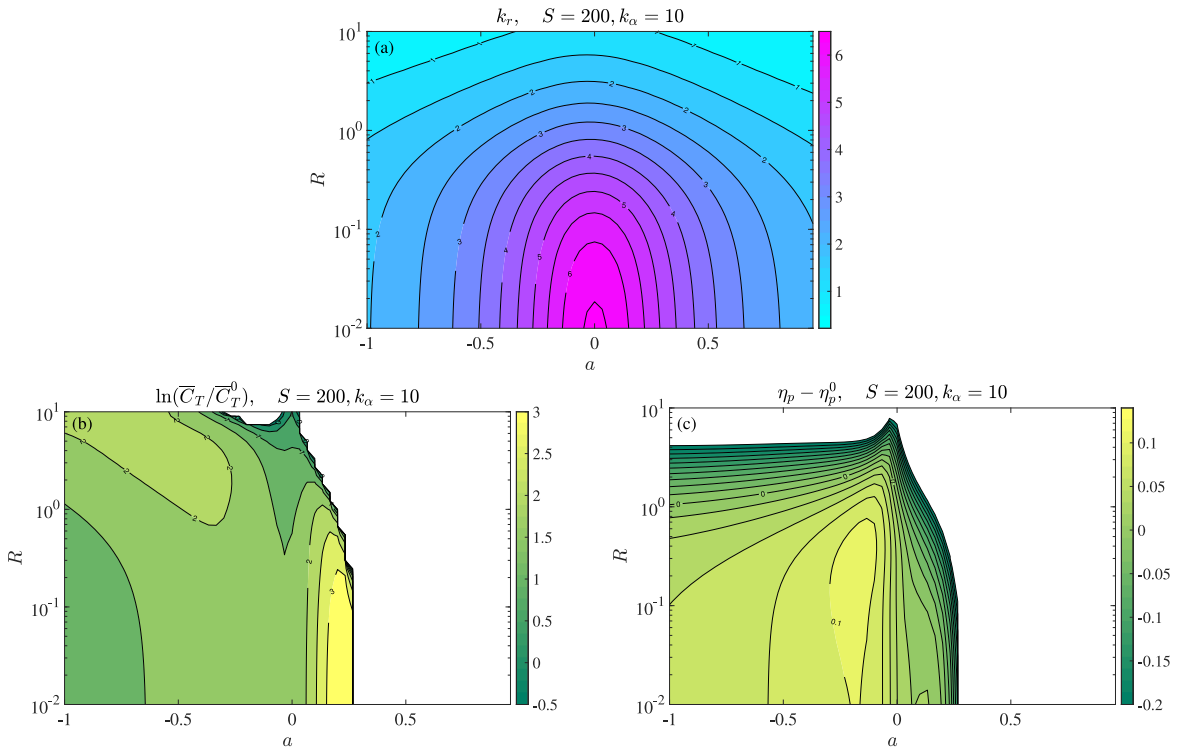


Fig. 12. Contours of resonant frequency k_r minimizing $|\det(\mathbf{A})|$ in the (a, R) plane (a), and the corresponding thrust (b) and efficiency (c) amplifications for $k = k_r$, when $S = 200$ and $k_\alpha = 10$. Negative values of \overline{C}_T in (a) and values of $\eta_p - \eta_p^0 < -0.2$ in (b) have been whited out.

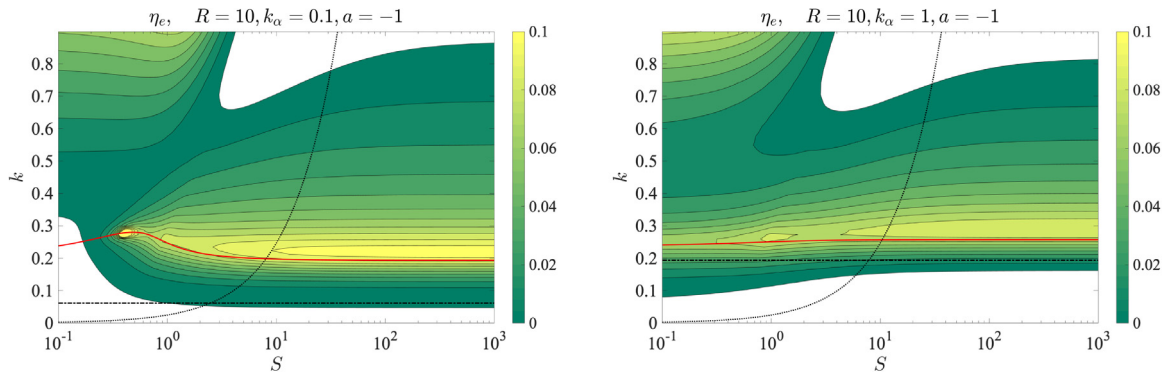


Fig. 13. Energy harvesting efficiency $\hat{\eta}_e$ as a function of stiffness S and frequency k for forced heaving motion with passive pitching at the leading edge ($a = -1$) of a flexible foil with mass ratio $R = 10$ for two spring stiffness, $k_\alpha = 0.1$ (left) and $k_\alpha = 1$ (right). $b_\alpha = 1$ and $b_h = 0$. The continuous lines correspond to the natural frequency of the system minimizing $|\det(\mathbf{A})|$, the dashed-and-dotted lines correspond to (27) and the dotted lines to (29).

see how the efficiency varies with S . The results are plotted in Fig. 13 in the stiffness–frequency plane for the same two values of the spring stiffness considered in Fig. 7, namely $k_\alpha = 0.1$ and 1, also pivoting about the leading edge ($a = -1$), and with the energy harvested only by the torsional damper ($b_h = 0$ and $b_\alpha = 1$).

In addition to the mode associated to the torsional spring, which coincides with the one shown in Fig. 7 for $R = 10$ when $S \rightarrow \infty$, there appears a higher frequency bending mode. However, it does not correspond to any local minima of $|\det(\mathbf{A})|$, nor it is well captured by the corresponding bending mode without FSI, shown in Fig. 13 with dotted lines. In contrast, the other lower frequency (spring) mode is very well captured by the resonant frequency $k = k_r$ that minimizes $|\det(\mathbf{A})|$, also shown in Fig. 13 by continuous lines, and it is slightly underpredicted by the corresponding resonant frequency k_{r0} without FSI, given by Eq. (27) and shown in Fig. 13 with dashed-and-dotted lines. As it happened for the rigid-foil case, this quiescent resonant frequency k_{r0} provides a good estimate of the lower frequency bound above

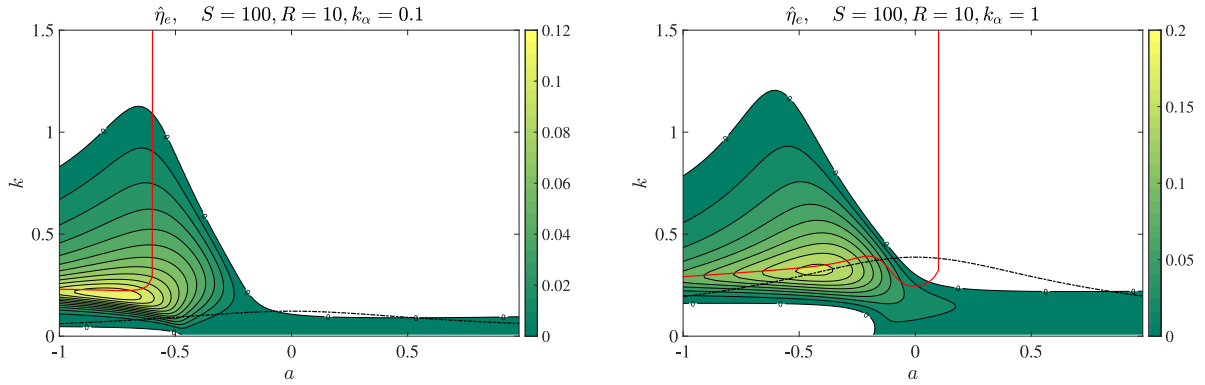


Fig. 14. Energy harvesting efficiency $\hat{\eta}_e$ as a function of frequency k and pivot point a for forced heaving motion with passive pitching of a flexible foil with stiffness $S = 100$ and mass ratio $R = 10$ for two spring stiffness, $k_{\alpha} = 0.1$ (left) and $k_{\alpha} = 1$ (right). $b_{\alpha} = 1$ and $b_h = 0$. The continuous lines correspond to the first natural frequency of the system minimizing $|\det(\mathbf{A})|$, while the dashed lines represent this frequency without FSI and $b_{\alpha} = 0$ (Eq. (27)).

which energy can be extracted from the current for given R , k_{α} and a . When the FSI is taken into account, k_r depends also on the foil stiffness S .

The maximum in the energy harvesting efficiency is not necessarily obtained for the rigid-foil case ($S \rightarrow \infty$), existing some local maxima at relatively low stiffness that depends on the remaining parameters. In the cases plotted in Fig. 13, these local maxima of $\hat{\eta}_e$ are for S about unity or slightly smaller. However, in both cases the efficiency increases when S is larger than about 100 when operating close to the natural frequency. To see how this maximum evolves with the pivot point location, we plot in Fig. 14 the efficiency in the frequency–stiffness plane for $R = 10$, $S = 100$ and the same values of k_{α} of Fig. 13. In both cases, the maxima in the efficiency remain if the pivot point is not too far from the leading edge, disappearing when the pivot point location reaches the quarter-chord length, or a slightly downstream, depending on k_{α} , a phenomenon marked by an abrupt increase of the first natural frequency predicted by the minimum of $|\det(\mathbf{A})|$. When $k_{\alpha} = 1$, the maximum efficiency is reached for $a \simeq -0.4$ and $k \simeq k_r \simeq 0.33$, and it is almost twice that the maximum for $k_{\alpha} = 0.1$, reached for $a \simeq -0.8$ and $k \simeq 0.21$.

5. Conclusions

A general formulation for the fluid–structure interaction and the aerodynamic performance of a foil with prescribed harmonic heaving motion and with passive pitching and passive chordwise flexibility about an arbitrary pivot point has been developed from the two-dimensional Euler–Bernoulli beam equation for small amplitudes coupled with fluid forces and moments obtained from the vortex impulse theory in the linearized potential limit by Alaminos-Quesada and Fernandez-Feria (2020). The formulation provides the pitch amplitude and its phase, and the flexural amplitude its phase, from a system of two complex, algebraic linear equations whose absolute value of its denominator determinant provides the (first) natural frequency of the foil–fluid system. A third algebraic equations determines the input force that generates the prescribed heave, and therefore the input power to compute the efficiency of the flapping-foil system. Besides the torsional spring at the pivot point, which allows for the passive pitching, the formulation may include a linear spring and two dampers, linear and torsional, to model also a flapping-foil turbine with passive pitching and deformation, in addition to the flapping-foil propulsor. Thus, the performance of these two quite different flapping-foils devices can be analyzed using the same set of algebraic equations in the limit of high Reynolds number and small flapping amplitudes. The maximum thrust in the propulsion system and the maximum energy harvesting efficiency are always found at, or near, the natural frequency of the system, but the maximum propulsive efficiency is not related to that frequency.

The results for the propulsive performance of rigid and flexible uniform foils coincide with previous ones by Moore (2014, 2015) when the pivot point is located at the leading edge, in spite of the quite different formulations. Thus, for instance, it is shown that the maximum thrust enhancement when pivoting at the leading edge is generated with a uniform foil in the limit of infinite stiffness. Here the results are extended to arbitrary pivot point locations and to general density and stiffness distributions along the foil. It is obtained that the maximum thrust amplification is reached for pivots just upstream of the quarter-chord point, and for mass ratios of the order unity, while the maximum efficiency enhancement is obtained when pivoting just upstream of the mid-chord point and for mass ratios lower than unity. The thrust force obtained here for rigid foils and different pivot point locations are also in quite good agreement with very recent experimental results by Asselin and Williamson (2019).

The present results for rigid-foil energy harvesting efficiency are in good agreement with recent numerical results by Boudreau et al. (2019a,b) when different parameters, including the pivot point location, are varied, in spite of the fact that their simulations are not for small flapping amplitudes. Now, contrary to the propulsion problem, the best efficiency

is obtained using foils with sufficiently large mass ratios, but also operating at its corresponding natural frequency, which here is obtained algebraically in terms of all the relevant parameters governing the problem. This natural frequency is always larger than that corresponding to the flapping-foil system without considering FSI, which in the present results approximately marks the threshold frequency above which the system may work as an energy harvester for a given set of parameters, in qualitative agreement with the numerical results of Boudreau et al. The effect of flexibility on the passive-pitch energy harvester is also analyzed, finding that the best performance is not always reached for very large stiffness, but for dimensionless stiffness of order unity, with the foil pivoting between the leading edge and the quarter-chord point, and for dimensionless mass ratios of order ten or larger.

Although the present linear approach does not cover the large pitching motions that have been illustrated to be optimal in the energy harvesting scenario, nor the non-linear coupling effects between passive pitching and structural bending which is known to be beneficial for thrust, we believe that the general analytical expressions developed here allow for a wide parametric survey and analysis of these two physical problems. Also, the findings for the particular flapping-foil configurations, which have been selected in part to compare with previous numerical and experimental results, may be of interest as a first guide in the design of some specific aerial or aquatic thrusters, and energy harvesting devices, based on flapping flexible foils with passive pitching. But many other potential applications of the method to problems that are physically valuable in both scenarios can be analyzed. In particular, since the first natural frequency of the system is well predicted by the present analytical formulation, we believe it may be quite useful as a guide for numerical simulations of the full nonlinear flapping problem searching for the optimal combinations of the wide set of parameters involved, such as the pivot point location, bending and torsional stiffnesses, mass ratio, center of mass, and moment of inertia, among others. Only the effects of just a few of these parameters in both scenarios have been analyzed in the examples considered here.

Declaration of competing interest

The authors declare that they have no known competing financial interests or personal relationships that could have appeared to influence the work reported in this paper.

Acknowledgments

This research has been supported by the *Ministerio de Ciencia, Innovación y Universidades* of Spain (DPI2016-76151-C2-1-R and PID2019-104938RB-I00) and from the Junta de Andalucía, Spain (UMA18-FEDER-JA-047 and P18-FR-1532).

Appendix A. Lift, moment and flexural coefficients

The following expressions for the coefficients corresponding to the quartic foil's deflection (11) are derived in Fernandez-Feria and Alaminos-Quesada (2021). Here are written in a more straightforward form in terms of $h(t)$, $\alpha(t)$, $d(t)$ and their temporal derivatives:

$$C_L(t) = \pi \left[-\ddot{h} - a\ddot{\alpha} + \dot{\alpha} + A_{l2}(a)\ddot{d} + A_{l1}(a)\dot{d} \right] + c(k)\Gamma_0(t), \tag{A.1}$$

$$C_M(t) = \frac{\pi}{2} \left[a\dot{h} + \left(a^2 + \frac{1}{8} \right) \ddot{\alpha} + \left(\frac{1}{2} - a \right) \dot{\alpha} + A_{m2}(a)\ddot{d} + A_{m1}(a)\dot{d} + A_{m0}(a)d \right] - \frac{1}{2} \left(\frac{1}{2} + a \right) c(k)\Gamma_0(t), \tag{A.2}$$

$$C_F(t) = \pi \left[- \left(a^2 + \frac{1}{4} \right) \ddot{h} - a \left(a^2 + \frac{1}{2} \right) \ddot{\alpha} + a(a-1)\dot{\alpha} + A_{f2}(a)\ddot{d} + A_{f1}(a)\dot{d} + A_{f0}(a)d \right] + \left(\frac{1}{2} + a + a^2 \right) c(k)\Gamma_0(t), \tag{A.3}$$

where

$$\Gamma_0(t) = -2\pi \left[\dot{h} + \left(a - \frac{1}{2} \right) \dot{\alpha} - \alpha + A_{g1}(a)\dot{d} + A_{g0}(a)d \right] \tag{A.4}$$

is the quasi-steady circulation, with

$$c(k) = \frac{H_1^{(2)}(k)}{iH_0^{(2)}(k) + H_1^{(2)}(k)} = \mathcal{F}(k) + i\mathcal{G}(k) \tag{A.5}$$

Theodorsen's function (Theodorsen, 1935), and $H_n^{(2)}(z) = J_n(z) - iY_n(z)$, $n = 0, 1$, Hankel's function of the second kind and order n , related to the Bessel functions of the first and second kind $J_n(z)$ and $Y_n(z)$ (Olver et al., 2010), and where the following functions of the pivot point location a have been defined:

$$A_{l2} = -\frac{13 + 48a^2 - 64a^3 + 24a^4}{48(1-a)^2}, \quad A_{l1} = \frac{3 + 12a - 12a^2 + 4a^3}{6(1-a)^2}, \quad (\text{A.6})$$

$$A_{m2} = \frac{2 + 25a - 12a^2 + 52a^3 - 64a^4 + 24a^5}{48(1-a)^2}, \quad A_{m1} = \frac{-9 + 12a - 72a^2 + 56a^3 - 16a^4}{24(1-a)^2}, \quad (\text{A.7})$$

$$A_{m0} = -\frac{3}{4(1-a)^2}, \quad A_{f2} = -\frac{35 + 32a + 392a^2 - 320a^3 + 496a^4 - 512a^5 + 192a^6}{384(1-a)^2}, \quad (\text{A.8})$$

$$A_{f1} = \frac{1 + 8a - 18a^2 + 48a^3 - 32a^4 + 8a^5}{12(1-a)^2}, \quad A_{f0} = \frac{7 + 18a}{12(1-a)^2}, \quad (\text{A.9})$$

$$A_{g1} = \frac{15 - 48a + 96a^2 - 80a^3 + 24a^4}{48(1-a)^2}, \quad A_{g0} = \frac{3 - 24a + 24a^2 - 8a^3}{12(1-a)^2}. \quad (\text{A.10})$$

Note that since Theodorsen's function is a complex quantity, so do are expressions (A.1)–(A.4) for the coefficients, where we also use the complex forms of the kinematics (22)–(24), so that one has to take the real part of these expressions to obtain real-valued quantities. However, as explained in Section 3, we use the complex Eqs. (13) and (14) to obtain the pitch and flexural deflection amplitudes and phases, a_0 , d_m , ϕ and ψ , directly.

Appendix B. Coefficients in Eq. (25)

$$A_{11} = I_a k^2 - 2k_\alpha - 2b_\alpha ik + A_{11}^F, \quad (\text{B.1})$$

$$A_{12} = -J_d k^2 - \frac{16}{3} \frac{a}{(1-a)^2} S + A_{12}^F, \quad (\text{B.2})$$

$$A_{21} = I_d k^2 + A_{21}^F, \quad (\text{B.3})$$

$$A_{22} = -K_d k^2 + \frac{16}{3} \frac{a^2 + \frac{1}{3}}{(1-a)^2} S + A_{22}^F, \quad (\text{B.4})$$

$$b_1 = m(x_0 - a)k^2 + b_1^F, \quad (\text{B.5})$$

$$b_2 = I_a k^2 + b_2^F, \quad (\text{B.6})$$

where the superscript F refers to the contributions to these coefficients from the fluid–structure interaction (i.e., from C_M and C_F). Using the expressions of C_M and C_F in Appendix A, these contributions can be written as

$$A_{11}^F = -\pi \left\{ \left(\frac{1}{2} - a \right) ik - \left(a^2 + \frac{1}{8} \right) k^2 + \mathcal{C}(k)(1 + 2a) \left[\left(a - \frac{1}{2} \right) ik - 1 \right] \right\}, \quad (\text{B.7})$$

$$A_{12}^F = -\pi \left\{ -A_{m2} k^2 + A_{m1} ik + A_{m0} + \mathcal{C}(k)(1 + 2a) [A_{g1} ik + A_{g0}] \right\}, \quad (\text{B.8})$$

$$A_{21}^F = \pi \left\{ -a \left(a^2 + \frac{1}{2} \right) k^2 + a(1-a) ik + \mathcal{C}(k)(2a^2 + 2a + 1) \left[\left(a - \frac{1}{2} \right) ik - 1 \right] \right\}, \quad (\text{B.9})$$

$$A_{22}^F = \pi [A_{f2} k^2 - A_{f1} ik - A_{f0} + \mathcal{C}(k)(2a^2 + 2a + 1) (A_{g1} ik + A_{g0})], \quad (\text{B.10})$$

$$b_1^F = -\pi a k^2 + \pi \mathcal{C}(k)(1 + 2a) ik, \quad (\text{B.11})$$

$$b_2^F = \pi \left(a^2 + \frac{1}{4} \right) k^2 - \pi \mathcal{C}(k)(2a^2 + 2a + 1) ik. \quad (\text{B.12})$$

Appendix C. Functions for the time-averaged thrust coefficient

The functions $t_h(k)$, $t_{hp}(k, a, \phi)$, $t_p(k, a)$, $t_{dh}(k, a, \psi)$, $t_{pd}(k, a, \phi, \psi)$ and $t_d(k, a)$ appearing in the time-averaged thrust coefficient (34) can be derived using a similar procedure to that described in Alaminos-Quesada and Fernandez-Feria (2020) for a quadratic foil deflection z_s . The resulting expressions can be written as follows:

$$t_h = -2\mathcal{G}_1, \tag{C.1}$$

$$t_{hp} = \left[4 \left(\frac{1}{4} - a \right) \mathcal{G}_1 k + \pi (k g_1^R - \mathcal{G}) \right] \cos(\phi) + \left[\pi (\mathcal{F} + k g_1^I) + \mathcal{F}_1 k + 4\mathcal{G}_1 \right] \sin(\phi), \tag{C.2}$$

$$t_p = \left(\frac{1}{2} - a \right) k \left[2a\mathcal{G}_1 k + \pi (\mathcal{G} - k g_1^R) \right] - \pi (\mathcal{F} + k g_1^I) - \mathcal{F}_1 k - 2\mathcal{G}_1, \tag{C.3}$$

$$t_{hd} = \left[\pi (A_{d0}^I - kA_{d1}^R - D\mathcal{G}) - 2A\mathcal{G}_1 k + \frac{3}{2}(E - J) \left(\pi\mathcal{G} - \frac{\mathcal{G}_1 k}{2} \right) - Q \left(\mathcal{F}_1 - \frac{\mathcal{G}_1 k}{2} + \frac{\pi\mathcal{G}}{2} \right) \right] \cos(\psi) + \left[\pi (-A_{d0}^R - kA_{d1}^I + D\mathcal{F}) - 2A\mathcal{F}_1 k + \frac{3}{2}(E - J) \left(-\frac{\mathcal{F}_1 k}{2} - \pi\mathcal{F} \right) + Q \left(\frac{\mathcal{F}_1 k}{2} + \frac{\pi\mathcal{F}}{2} + \mathcal{G}_1 \right) \right] \sin(\psi), \tag{C.4}$$

$$t_{pd} = \left\{ \pi \left[\left(\frac{1}{2} - a \right) k (-A_{d0}^I + kA_{d1}^R + D\mathcal{G}) + A_{d0}^R + kA_{d1}^I - D\mathcal{F} \right] + 2Ak \left[-a\mathcal{G}_1 k + \mathcal{F}_1 + \frac{\pi}{2} (k g_1^R - \mathcal{G}) \right] + \frac{3}{2}(E - J) \left[\pi \left(\mathcal{F} - \left(\frac{3}{4} - a \right) \mathcal{G} k + \frac{k^2}{4} g_1^R \right) + \frac{k}{2} (\mathcal{F}_1 - a\mathcal{G}_1 k) \right] - Q \left[\pi \left(\frac{k}{2} (a - 1)\mathcal{G} + \mathcal{F} + \frac{k g_1^I}{2} + \frac{k^2}{4} g_1^R \right) + \left(a + \frac{1}{2} \right) \mathcal{F}_1 k + \mathcal{G}_1 \left(1 - \frac{ak^2}{2} \right) \right] \right\} \cos(\phi - \psi) + \left\{ \pi \left[-\left(\frac{1}{2} - a \right) k (A_{d0}^R + kA_{d1}^I - D\mathcal{F}) - A_{d0}^I + kA_{d1}^R + D\mathcal{G} \right] + 2Ak \left(a\mathcal{F}_1 k + \frac{\pi}{2} (\mathcal{F} + k g_1^I) + \mathcal{G}_1 \right) + \frac{3}{2}(E - J) \left[\frac{k}{2} (a\mathcal{F}_1 k + \mathcal{G}_1) - \pi \left(\mathcal{G} + \left(\frac{1}{4} - a \right) \mathcal{F} k - \frac{k^2}{4} g_1^I \right) \right] - Q \left[\frac{\pi}{2} k \left(a\mathcal{F} + \frac{k g_1^I}{2} - g_1^R \right) - \mathcal{F}_1 \left(1 - \frac{ak^2}{2} \right) + \left(a + \frac{1}{2} \right) \mathcal{G}_1 k \right] \right\} \sin(\phi - \psi), \tag{C.5}$$

$$t_d = \frac{\pi}{4} \left\{ Q \left[-kA_{d0}^I + 2A_{d0}^R + 2kA_{d1}^I + k^2 A_{d1}^R - 2AGk + D(\mathcal{G}k - 2\mathcal{F}) + (E - J) \left(3\mathcal{F} - \frac{9\mathcal{G}k}{4} \right) \right] + k \left(4A + \frac{3E}{2} - \frac{3J}{2} \right) \left[A_{d0}^I - kA_{d1}^R + \mathcal{G} \left(-D + \frac{3E}{2} - \frac{3J}{2} \right) \right] + Q^2 \left(\frac{\mathcal{G}k}{2} - \mathcal{F} \right) \right\}, \tag{C.6}$$

where the following functions of the pivot point location a have been used:

$$A(a) = a^2 \left(1 + \frac{2a}{3(1-a)} + \frac{a^2}{6(1-a)^2} \right), \quad B(a) = 2a \left(1 + \frac{a}{1-a} + \frac{a^2}{3(1-a)^2} \right), \tag{C.7}$$

$$D(a) = 1 + \frac{2a}{1-a} + \frac{a^2}{(1-a)^2}, \quad E(a) = \frac{2}{3(1-a)} \left(1 + \frac{a}{1-a} \right), \quad J(a) = \frac{1}{6(1-a)^2}, \tag{C.8}$$

$$Q(a) = 2B(a) - 2D(a) + 3E(a) - 3J(a); \tag{C.9}$$

$\mathcal{F}(k)$ and $\mathcal{G}(k)$ are the real and imaginary parts of Theodorsen's function (A.5), and likewise $\mathcal{F}_j(k)$ and $\mathcal{G}_j(k)$, $j = 1, 2, 3$, in relation to the complex functions $C_j(k)$, defined as,

$$C_1(k) = \frac{\frac{1}{k} e^{-ik}}{iH_0^{(2)}(k) + H_1^{(2)}(k)}, \quad C_2(k) = \frac{H_2^{(2)}(k)}{iH_0^{(2)} + H_1^{(2)}(k)}, \quad C_3(k) = \frac{Y_0(k) - ij_2(k) + iH_1^{(1)}(k)}{iH_0^{(2)} + H_1^{(2)}(k)}, \tag{C.10}$$

and $g_j^R(k)$ and $g_j^I(k)$, $j = 0, 1, 2, 3, 4$, in relation to the complex functions

$$g_0(k) = \frac{-2i}{\pi} C_1(k), \quad g_1(k) = -\frac{2}{\pi k} (1 + ik) C_1(k) - \frac{i}{k} C(k), \quad g_2(k) = -\frac{1}{k} C_2(k) + \left(\frac{2i}{k^2} - \frac{2 + ik}{k} \right) C_1(k), \tag{C.11}$$

$$g_3(k) = \frac{3Y_2(k) - kY_1(k) + ij_3(k) - ij_2(k)}{k^2 [iH_0^{(2)} + H_1^{(2)}(k)]} + \frac{6}{\pi k} (1 + ik) \left(\frac{2}{k^2} - 1 \right) C_1(k), \tag{C.12}$$

$$g_4(k) = \frac{1}{iH_0^{(2)} + H_1^{(2)}(k)} \left\{ \frac{1}{k^2} [kJ_4(k) - 3J_3(k)] + \frac{ik}{4} G_{1,3}^{2,0} \left(\frac{k^2}{4} \mid -3, 0, -\frac{3}{2} \right) \right\}$$

$$+ \frac{2}{\pi} \left[\frac{24}{k^4}(k-i) - \frac{4}{k^2}(k-3i) - i \right] c_1(k), \quad (\text{C.13})$$

with J_ν and Y_ν the Bessel functions of the first and second kind, respectively, of order ν , and $G_{p,q}^{m,n}(z|\mathbf{a}_p; \mathbf{b}_q)$ the Meijer G-function (Olver et al., 2010). Finally, $A_{dj}^R(k, a)$ and $A_{dj}^I(k, a)$, $j = 0, 1$, are the real and imaginary parts of the functions

$$A_{d0}(k, a) = -Bg_0 + D[1 + 2g_1(k) - c(k)] - E \left[\frac{1}{2} + 3g_2 + \frac{C}{2} \right] + J \left[4g_3 + \frac{C}{2} + \frac{C_3}{k} \right], \quad (\text{C.14})$$

$$A_{d1}(k, a) = Ag_0 - Bg_1 + Dg_2 - E \left[g_3 - \frac{i}{2k}C \right] + J \left[g_4 - \frac{C_2}{2k} \right]. \quad (\text{C.15})$$

References

- Alaminos-Quesada, J., Fernandez-Feria, R., 2020. Propulsion of a foil undergoing a flapping undulatory motion from the impulse theory in the linear potential limit. *J. Fluid Mech.* 883 (A19), 1–24.
- Alben, S., 2008. Optimal flexibility of a flapping appendage in an inviscid fluid. *J. Fluid Mech.* 614, 355–380.
- Alben, S., Witt, C., Baker, T.V., Anderson, E., Lauder, G.V., 2012. Dynamics of freely swimming flexible foils. *Phys. Fluids* 24, 051901.
- Anevavi, D.E., Filippas, E.S., Karperaki, A.E., Belibassakis, K.A., 2020. A non-linear BEM-FEM coupled scheme for the performance of flexible flapping-foil thrusters. *J. Mar. Sci. Eng.* 8, 56.
- Asselin, D., Williamson, C.H.K., 2019. Addition of passive dynamics to a heaving airfoil to improve performance in the report by c.h.k. In: Williamson 'Fluid-Structure Interactions Employing Cyber-Physical Fluid Dynamics. Tech. Rep. AFRL-AFOSR-VA-TR-2019-0114, Air Force Research Laboratory.
- Boudreau, M., Gunther, K., Dumas, G., 2019a. Free-pitching flapping-foil turbines with imposed sinusoidal heave. *J. Fluids Struct.* 90, 110–138.
- Boudreau, M., Gunther, K., Dumas, G., 2019b. Investigation of the energy-extraction regime of a novel semi-passive flapping-foil turbine concept with a prescribed heave motion and a passive pitch motion. *J. Fluids Struct.* 84, 368–390.
- Fernandez-Feria, R., 2016. Linearized propulsion theory of flapping airfoils revisited. *Phys. Rev. Fluids* 1, 084502.
- Fernandez-Feria, R., 2017. Note on optimum propulsion of heaving and pitching airfoils from linear potential theory. *J. Fluid Mech.* 826, 781–796.
- Fernandez-Feria, R., Alaminos-Quesada, J., 2021. Analytical results for the propulsion performance of a flexible foil with prescribed pitching and heaving motions and passive small deflection. *J. Fluid Mech.* 910, A43.
- Floryan, D., Rowley, C.W., 2018. Clarifying the relationship between efficiency and resonance for flexible inertial swimmers. *J. Fluid Mech.* 853, 271–300.
- Floryan, D., Rowley, C.W., 2020. Distributed flexibility in inertial swimmers. *J. Fluid Mech.* 888, A24–1–37.
- Garrick, I.E., 1936. Propulsion of a flapping and oscillating airfoil. Tech. Rep. TR 567, NACA.
- Lighthill, M.J., 1969. Hydromechanics of aquatic animal propulsion. *Ann. Rev. Fluid Mech.* 1, 413–449.
- Michelin, S., Lewellyn Smith, S.G., 2009. An unsteady point vortex method for coupled fluid-solid problems. *Theor. Comput. Fluid Dyn.* 23, 127–153.
- Moore, M.N.J., 2014. Analytical results on the role of flexibility in flapping propulsion. *J. Fluid Mech.* 757, 599–612.
- Moore, M.N.J., 2015. Torsional spring is the optimal flexibility arrangement for thrust production of a flapping wing. *Phys. Fluids* 27, 091701.
- Moore, M.N.J., 2017. A fast Chebyshev method for simulating flexible-wing propulsion. *J. Comput. Phys.* 345, 792–817.
- Olver, F.W.J., Lozier, D.W., Boisvert, R.F., Clark, C.W. (Eds.), 2010. *NIST Handbook of Mathematical Functions*. Cambridge University Press, Cambridge, (UK).
- Theodorsen, T., 1935. General theory of aerodynamic instability and the mechanism of flutter. Tech. Rep. TR 496, NACA.
- Xiao, Q., Zhu, Q., 2014. A review on flow energy harvesting based on flapping foils. *J. Fluids Struct.* 46, 174–191.
- Young, J., Lai, J.C.S., Platzer, M.F., 2014. A review of progress and challenges in flapping foil power generation. *Prog. Aero. Sci.* 67, 2–28.